A CMOS SWITCHED CAPACITOR FILTER BASED POTENTIOMETRIC READOUT CIRCUIT FOR CHEMFET SENSOR

by

REVATHY PERUMALSAMY

Presented to the Faculty of the Graduate School of

The University of Texas at Arlington in Partial Fulfillment

of the Requirements

for the Degree of

MASTER OF SCIENCE IN ELECTRICAL ENGINEERING

THE UNIVERSITY OF TEXAS AT ARLINGTON

December 2018

ACKNOWLEDGEMENTS

I am thankful to my advisor Dr. Sungyong Jung for guiding me through to successfully complete this thesis defense. Along with engineering and research capabilities he has groomed me to look at ideas with deeper insight and conviction, since the fall of 2016. He has been persistent, motivating and encouraging. If not for him, it would not have been possible for me to submit an integrated circuit design in 0.18µm technology for fabrication and test it as a Master's student. He owns the credit for all that I have achieved today and for making me a good circuit designer.

I also thank, Dr. Yuze Sun and Dr. Schizas Ioannis for their consent and time to serve on my thesis defense committee and evaluate my work. Special thanks to Dr. Yuze Sun for the lectures on biomedical sensor, which helped me in the research work.

I am lucky to have worked with the best minds of AMIC lab and thank them all lab members

Finally I thank my parents and I am most grateful to them for giving me an opportunity to pursue my Master's at University of Texas at Arlington. They have supported and motivated with their love in all my endeavors. Thanks to all my friends, well-wishers and former colleagues at Texas Instruments, Wipro Technologies and Tessolve DTS Inc. for providing me with much needed moral and financial support to complete this work successfully!!

November 26, 2018

ABSTRACT

A CMOS SWITCHED CAPACITOR FILTER BASED POTENTIOMETRIC READOUT CIRCUIT FOR CHEMFET SENSOR

Revathy Perumalsamy, M.S.

The University of Texas at Arlington, 2018

Supervising Professor: Sungyong Jung

There are wide ranges of potentiometric sensors available for chemical sensing. The latest implementation of these sensors is CHEM resistors. In real time environment for an in-vivo application area, noise and power are the important factors. Though the selectivity of CHEM resistors improved with recent technological developments analog front end measurement circuits are always the limiting factor. Without compromising the performance parameters like gain and op-swing it is a challenge to improve the noise and power. Noise and power are the two factors which always require improvement. Also, there is trade-off between noise and power which needs to be balanced. The fundamental noise generated by the device is a challenge to handle. CMOS amplifiers usage is limited by the non-deterministic noise like flicker, short and thermal.

It is seen that for potentiometric circuit the CDS is preferable for the sampled data circuits like the switched capacitor so that the base bad noise behavior is not made worse by noise aliasing. This eliminates the DC offset and drifts. Though we use CDS for various potentiometric measurements the filtering stage after the CDS limits the capability of noise reduction. Therefore in this thesis work the detailed analysis of CDS with switched capacitor based LP filter is introduced. The architecture used helps in accurate

measurement of pH, where the ratio of the chemical compound like sodium, potassium and chlorine is very critical.

The integrated circuits are designed using 0.18µm CMOS process. The layout of the designed chip is 3.8mm × 3.8mm. The design simulation is done with a load of 10pF and 100Hz input signal. The circuit operates with a supply range ±1.65V linearly reproduces the sensor output voltage ±1.5V. The noise measured with 1MHz sampling clock is 0.683µVrms and the power required for the system is 124.1µW.

TABLE OF CONTENTS

LIST OF ILLUSTRATIONS

List of Tables

CHAPTER 1

INTRODUCTION

The measure of acidity or alkalinity is very helpful in industries such as biomedical, chemical, agricultural and food. Even in our everyday life it plays an important role, for instance digestive system, oral health, metabolism, industrial process, and environment monitoring and soil health. The measure of acidity and alkalinity in any solution is also called as pH. The hydrogen ion concentration determines the acidic nature of a solution. Accurate measurement of pH helps to detect the imbalance and prevent permanent damage at an early stage. The study shows that pH of body fluids has relation to many chronic deceases. Monitoring pH and regulating it will prevent those chronic deceases at an early stage. For example, Intake of sugar causes acid formation in the mouth and this causes the pH to drop below 5.5 which triggers the demineralization of teeth. Tooth decay affects almost all age group of people which the cause for bad breath is, gum decease, tooth erosion and sensitivity. The risk factor of tooth decay depends on the tooth location, the pH of food that is consumed, frequent eating, inadequate brushing, aging, dry mouth and heart burn. Most of the time to protect the teeth it is advised to take a rinse and regular brushing. A pH level of 5.5 is an indication of healthy mouth. It is important to know that pH level drop facilitates the environment for cavities. Therefore, it is important to measure the fluctuations in the pH of the system. Sensitivity, accuracy, linearity and range of the sensor plays more important role in the pH measurement [1][2]. The sensitivity of the pH sensors is typically 59mV/pH [2].

Most common way of measuring the pH in electro chemistry is using a potentiometer. Potentiometer compares the potential developed by the hydrogen ion concentration in the solution with a known potential. This is done with the help of sensing electrode and a

reference electrode. The sensing electrode is made of Ag/AgCl or HCL, which are called glass electrodes and the reference electrode, is made of KCL or Hg_2Cl_2 or Hg. The electrode plays a key role in sensitivity, repeatability and accuracy of the sensor. Also, the solution for which the pH is measured is sensitive to temperature drift. To avoid this normally temperature compensation element would be added during pH measurement. Although glass electrodes provide more accurate and linear response, they are larger in diameter and very inconvenient in in-vivo applications. The latest development on ISFET proves that their performance is equivalent to glass electrodes. This leads to more compact and portable measuring devices. ISFET is more compact with wide range of pH measurement. The gate oxide can be modified by adding ion selective membrane which can be sensitive for specific compounds. The materials used for gate oxide are SiO_2, $Si3N_4$, Al_2O_3 and Ta_2O_5. The attachment of organic molecule can alter the functionality of ISFET which leads to the development of chemFET and bioFET. Also, these sensors are easy to fabricate with the CMOS technology. With the latest development in technology CMOS shows an advantageous nature towards the pH measurement. Its charge building nature and temperature coefficients are the most attractive features. Alongside the development in microelectronic circuits like op-amps shows amazing improvements over eliminating drifts and noise. The objective of a readout circuit for pH sensing using CMOS process should achieve low noise and low power. Also, it should cover the input range of the sensor and produce a linear output.

As pH sensors have a very low frequency output, the intrinsic noises generated by the transistors at the measurement circuit are very high. In recent trends, there are several analog front end architectures that are designed for potentiometric sensing. One such architecture is the Instrumentation amplifier with programmable gain is used for bio potential application [25] with the supply of 0.5V. Though the application archives a better

noise performance, for the operation range of 0.5V the noise generated is relatively high. But the switched capacitor based trans-impedance amplifier [22] architecture proves to use a supply range of 3V the noise performance of the circuit is not satisfactory. There are other biomedical signal accusation architectures proposed [35, 36] where to improve the noise performance the voltage headroom is compromised. The latest potentiometric application that uses CVCC architecture [37, 26] meets the requirement of voltage head room that operates in a 3.3V supply range. Though readout circuits with improved technology can provide improved sensitivity, temperature and drift compensation, the noise performance is not considered in the study. Also, this architecture power consumption is relatively high which is not suitable for the in-vivo application. All the discussed architectures share a mutual interest of using CMOS technology for low frequency application. The 1/f otherwise called flicker noise in CMOS is larger at lower frequency. Flicker noise imposes a limitation in reducing the circuit area and power dissipation which is very critical for in-vivo application. Therefore the motivation of this work is to effectively measure the sensor output without any distortion and improve the noise performance further without compromising the power consumption. In this work, the application of pH sensing system with a background of electro chemistry, techniques used to measure pH and the latest trends are reviewed. A novel method to reduce the noise in the measurement is proposed at the end. The proposed circuit achieves low noise, high SNR with optimal power consumption.

This thesis is presented in five chapters,

Chapter 1 presents the motivation of pH sensing system with a background of its environmental application and its monitoring with the help of electro chemistry. The research objectives for this thesis are described.

Chapter 2 provides the review of electrochemistry, types of electro chemical sensors and then the types of electrochemical sensing techniques, their advantages over the other methods are discussed.

Chapter 3 presents the CMOS design that is proposed for the pH sensing system. The design of correlated double sampler, along with the novel switched capacitor based low pass filter is explained. This proposed design improves the noise performance of the circuit which is discussed further. The design is built in 0.18µm CMOS process and the post layout simulated results are compared with other existing architectures.

Chapter 4 concludes the thesis with architecture proposed in this work and how further improvements can be obtained.

CHAPTER 2

BACKGROUND

Electrochemistry works by detecting the changes in the analyte's content. The chemical components react with each other by electron transfer. The type of reaction and the rate at which the reaction happens depends on the potential difference between the reference and the sensing electrode. The electron transfer in the analyte happens at the surface of the electrode, this rate at which the electron transfer happens is analyzed by applying a time varying signal potential or forcing current on the reference electrode.

2.1 ELECTROCHEMISTRY

Electrochemistry is based on Faraday's discovery of equivalence that exists between electricity and chemistry. The electrode in a solution performs the role of a transducer between the chemical and electrical domains by either monitoring the chemical components in the solution or by generating new chemical components that will interact with the medium in a measurable way. Electrochemical reactions occur in a medium containing dissolved ions (electrolyte) which aid the current flow. Usually, the solvent-electrolyte combination chosen for use in electrochemical experiments are strong electrolytes (fully broken down into ions when dissolved in solvent). Current flow between the electrodes in electrochemical cells is a function of solution resistance of the electrolyte between the electrodes. The value of this resistance depends on the ionic conductivity of the electrolyte, and on the geometric arrangement of electrodes in the cell [39]. Generally, description of the chemical reaction can be inferred by observing the voltage-current characteristic of an electrode/solution and relating it to the system

knowledge. Hence, most of the electrochemistry methods deal with the interrelation between interfacial potential differences and thermodynamics of electrode reactions.

Redox reaction happens between two half cells, each cell has a different species (A, B) and an electrode. An ion porous membrane is used to separate the half-cell, thus allowing the flow of ions between the species. The electrodes if connected with wire allowing the charge build up at the surface of the electrode and thus electron flow will happen from lower potential to higher potential cell. This electron flow happens until the half cells arrives equilibrium.

In the electro-chemical cell, the reduction and oxidation happen when the analyte gains and loses electrons. The electrodes of the half-cell were the accumulation of the electron happens is anode always be at a lower potential. The electron flows from the anode to the cathode thus allowing the reduction to happen at the cathodic cell. This electro-chemical cell can also be called as galvanic or voltaic cell.

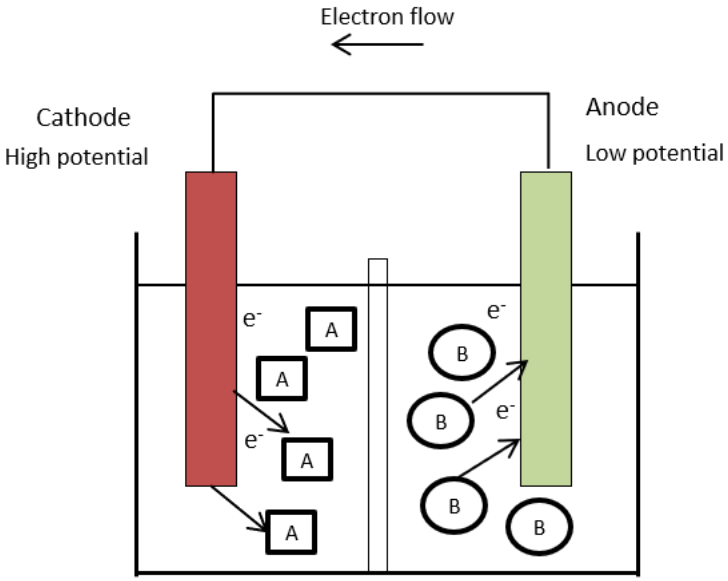

Figure 2-1: Electro chemical reaction in an electrolytic cell [39]

This electro-chemical cell reaction when carried out under controlled condition by applying an external potential forms the electrolytic cell as in figure 2-1. The process by which the reaction is controlled is called electrolysis. In electrolysis, the redox reaction happens with the help of electrical energy. In an electrolytic cell the oxidation and reduction still happens at the anode and the cathode, but to control the reaction a battery relates to its negative and positive terminal connecting to the cathode and anode respectively. Thus, providing the electrons to the cathode for reduction and allows to withdraw the electrons at the anode for oxidation. Equation (2.2) is an example for the oxidation and reduction of water,

Reduction: $2H_2O + 2e^- \rightarrow H_2 + 2OH^-$ (2.1)

Oxidation: $2H_2O - 4e^- \rightarrow O_2 + 4H^+$ (2.2)

Electrochemical cells are broadly divided into two sub-types, galvanic and electrolytic. In galvanic cells the reactions start spontaneously when the electrodes are connected via a conductor, while on the other hand an electrolytic cell Figure 2-2 requires a potential in excess of its operating cell potential (OCP) to be applied in order to drive an electrochemical process. The overall chemical reaction occurring in an electrochemical cell consists of two independent half-reactions describing the real chemical changes at each of the two electrodes. Each half-reaction responds to the interfacial potential difference at the corresponding electrode.

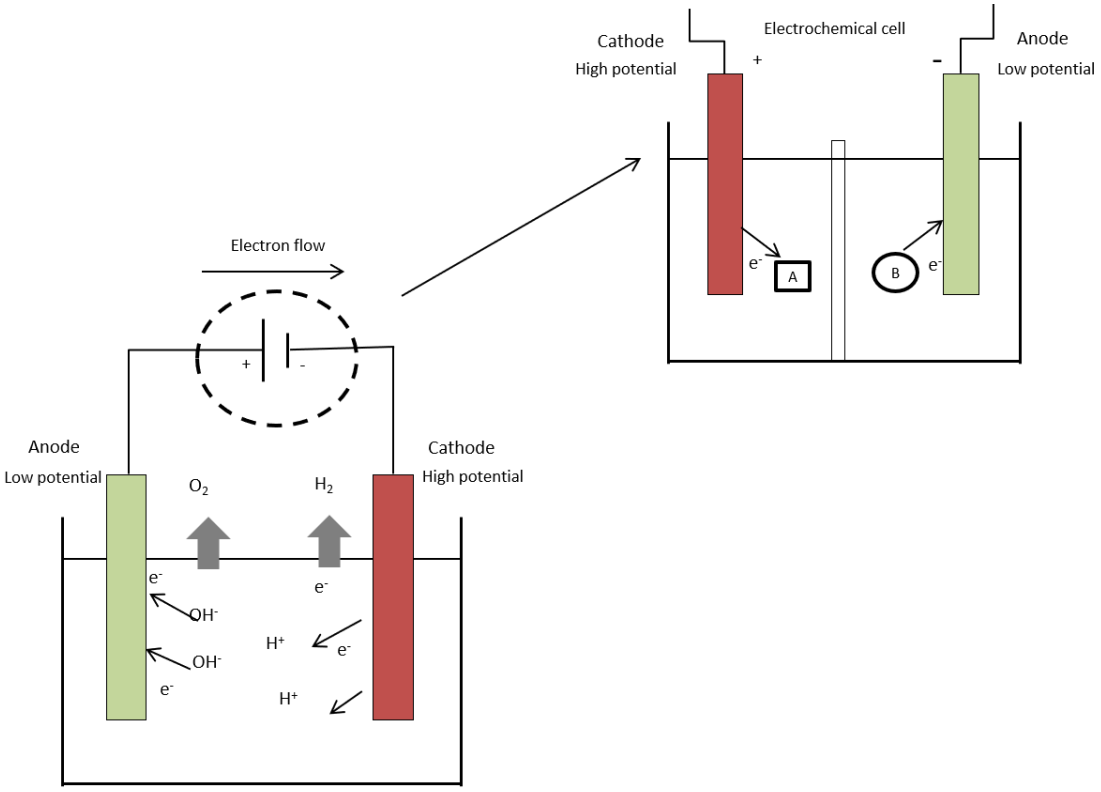

Figure 2-2: Electrolysis [39]

The electrical energy required for the redox to happen be equal to the Gibbs free energy in addition the loss caused by the heat dissipation. The amount of energy required for the oxidation and reduction is defined with the work function required to excite the electron from the fermi level of the species.

Where φ is the potential or work function required to gain or lose the electron for the species. Before applying the external potential, in electrolysis, the dynamic equilibrium is achieved when the rate at which the ions leaving and joining at the surface of the electrode is same. The final charge of the electrode depends on where the equilibrium

potential is situated in the energy band and decided were the solution is in positive or negative equilibrium. A salt solution is under negative equilibrium if the electrode has relatively lesser potential than reference solution and so is the amount of work or potential is less to observe a positive charge.

The solution containing M1 which has the energy function near to the zero reference tends gain the electron and reduces with a lower applied potential. Similarly, the solution with M2 content tends to lose the electron and oxidize easily than the M1 solution. Thus, the equilibrium potential remains the same for a salt solution. This equilibrium potential is important in calculating the free energy charge (ΔG) which determines the electrical energy required for the redox reaction as shown in equation (2.3). Where ΔG° is standard free energy, M and M^{+} is the effective concentration of the reduced form and oxidized for respectively.

$$\Delta G = \Delta G^{\circ} + RT\ln\left(\frac{[\text{reduced form}]}{[\text{oxidized form}]}\right) \tag{2.3}$$

$$\Delta G = \Delta G^{\circ} + RT\ln\left(\frac{M}{M^{+}}\right) \tag{2.4}$$

The Gibbs free energy is related to the EMF or potential of the electrode (E) using equation (2.5),

$$\Delta G = -nFE \tag{2.5}$$

Where, n is the number of electrons and F is faradays constant $64 * 10^{4} C/mol$. Thus, equating ΔG in equation (2.6) gives the electrode potential.

$$E = -\frac{\Delta G^{\circ}}{nF} - \frac{RT}{nF}\ln\left(\frac{[\text{reduced form}]}{[\text{oxidized form}]}\right) \quad (2.6)$$

$$E = E^{\circ} + \frac{RT}{nF}\ln\left(\frac{M^{+}}{M}\right) \quad (2.7)$$

Here - $\frac{\Delta G^{\circ}}{nF}$ is termed as the standard reduction potential.

Nernst equation is a mathematical way to determine the electrode potential due to the temperature, oxidized and reduced species. In the equation (2.7), R is a universal gas constant $8.31 \mathrm{JK^{-1}mol^{-1}}$, n is the number of electrons.

So, at T = 298.15K,

$$E = E^{\circ} + 0.059\log\left(\frac{M^{+}}{M}\right) \quad (2.8)$$

For calculating a single electron transfer of the oxidized and the reduced species M^{+} and M should be substituted with one.

The current flow at an electrode/electrolyte interface is mainly due to two kinds of processes faradaic and Non-faradaic. In faradaic process the charges are transferred at the electrode/electrolyte interface due to oxidation or reduction reactions. Therefore, the resulting current is called faradaic current and the electrodes through which this current flow is called charge-transfer electrodes. This depends mostly on two factors [39], [17]:

1. The rate at which the material moves from the bulk of the electrolyte to the electrode surface (this is called mass transfer).

2. The rate at which electrons transfer from the electrode to electrolyte and vice versa (this is called charge transfer).

Non-faradaic processes, such as adsorption and desorption can cause a transient current flow through the interface when the potential, electrode area, or solution composition changes [9]. Therefore, in an ideal sensor, the sensor current should have only the faradaic component and the non-faradaic component should be zero.

2.2 ELECTROCHEMICAL SENSING

As discussed in the basic of electro chemistry the simple electro chemical dell uses two electrodes. The electrode which is sensitive to the potential is working electrode. The second electrode is the counter electrode which acts as the reference for the working electrode. The counter electrode potential is supposed to be constant but, if the potential is not constant it is replaced with reference electrode and an auxiliary electrode. With this circuitry, three basic controlling mechanisms can be designed which abides ohms' law.

- Varying the resistance of the bulk with zero current in the counter/reference electrode and measuring the potential difference.
- Maintaining a constant current in the auxiliary electrode by changing the voltage at the counter/reference electrode.
- The signal from the reference electrode is fed through an impedance transformer which maintains constant input current but leaves the voltage unchanged.

The potentiometer, galvanometer and potentiostat are the corresponding circuit configuration used for the measurements of the above three methods. The configurations are described in the following sections.

2.2.1 POTENTIOMETER

If the tap key T is closed in figure 2-3 limits the current passing through the work electrode thus limiting the change of the analyte in the electro chemical cell. For example, passing a current of 10^{-9} A through the electrochemical cell for 1 s changes the concentrations of species in the cell by approximately 10–14 moles [Analytical chemistry].

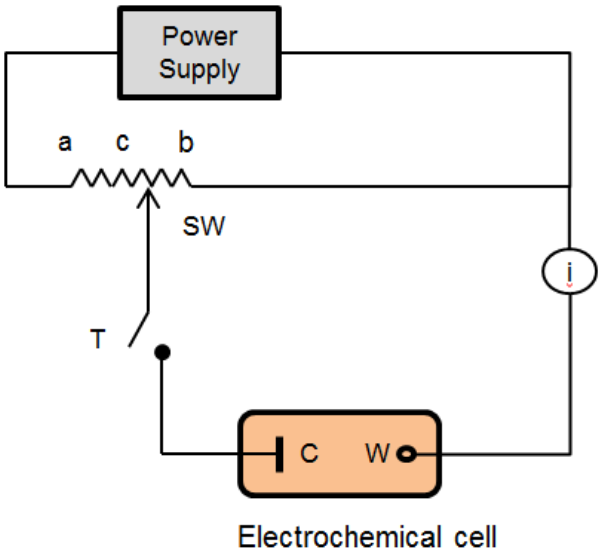

Figure 2-3 Potentiometer schematics [39]

$$i_{low} = \frac{E_{cell}}{R_{cb}} \tag{2.9}$$

$$\mathrm{E_{cell}} = \frac{\mathrm{R_{cb}}}{\mathrm{R_{ab}}} E_{\mathrm{ps}} \tag{2.10}$$

2.2.2 Galvano stat

The current flowing to the cell can be directly controlled. The reference electrode is just used to monitor the potential at the work electrode as shown in figure2-4.

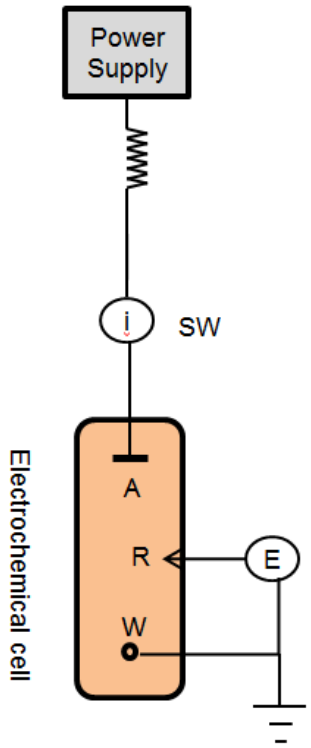

Figure 2-4 Galvano stat schematics [39]

$$\mathrm{i} = \frac{\mathrm{E_{ps}}}{\mathrm{R}} \approx constant \tag{2.11}$$

2.2.3 POTENTIOSTAT

Potentiostat controls the potential of the working electrode with the help of potentiometer in figure 2-5. The current flowing through the auxiliary and the working electrode loop is measured. If the potential of the profile is time dependent a pulse signal can be applied to the working electrode.

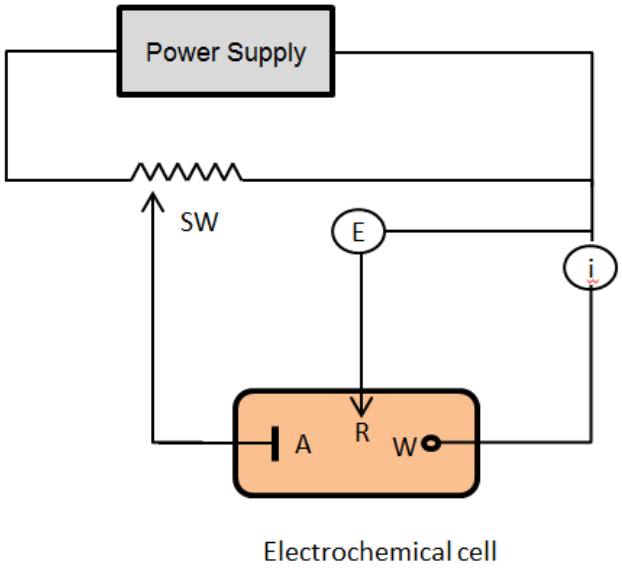

Figure 2-5 Potentiostat schematics [39]

Based on the three techniques discussed above the electro chemical reaction is classified into static and dynamic. In static, the current supplied to the analyte is not changed and the measurement of voltage is strait forward. While on the hand we have the combination of controlled potential and current for the dynamic process which

subdivides into different combinations. This subdivision can be generalized as coulometry, aerometry and voltammetry.

2.3 METHOD OF STUDY OF ELECTROCHEMICAL SENSORS

2.3.1 POTENTIOMETRY

Analyte is measured based on the electrical potential developed by a cell with very low current flow. Electrical potential that develops at the junction between two electrolyte solutions arises from unequal rates of diffusion of the cation and anion. Potentiometer blocks current between half cells and the EMF provides information on the free energy of the overall reaction. In potentiometric electrochemical cell the cathode potential changes with the anode. This makes anode as the reference electrode and cathode as the working electrode. The reference electrodes can be standard hydrogen electrode, calomel electrodes or Ag/AgCl electrodes. The working electrodes can be of membrane electrode, ion selective electrode, glass electrode, solid state ion selective electrode. Applications of this sensing circuit are concentration and activity, pH sensing.

Since the main application of the potentiometric circuitry shown in Figure 2-6 is to find the specific ion concentration and hence the selective electrodes are used as working electrodes. Metal electrodes and ion selective electrodes are used for the potentiometric measurements. Metal electrodes develop an electric potential by redox reaction at the metal surface. Ion-selective Electrodes selectively bind one type of ion to a membrane to generate an electric potential. Most of the biomedical application focuses on a specific compound in blood, meat, milk and so on. This is facilitating the use of ion-selective membranes as working electrode and hence the focus would be on the ISE. Suppose if

the membrane is glass, the ISE forms a concentration cell given due to the hydrogen ions on either side of the membrane and is partly influenced by alkaline ions present both in the glass and measured solution and not involve a redox process. H^+ diffuses into glass membrane and replaces Na^+ in hydrated gel region forming Ion-exchange equilibrium. Thus, calculating the potential difference by trapping the ions on the surface of the electrode using selective membranes helps in pH measurement.

$$E=\text{Constant}-\beta(0.05916)pH \tag{2.12}$$

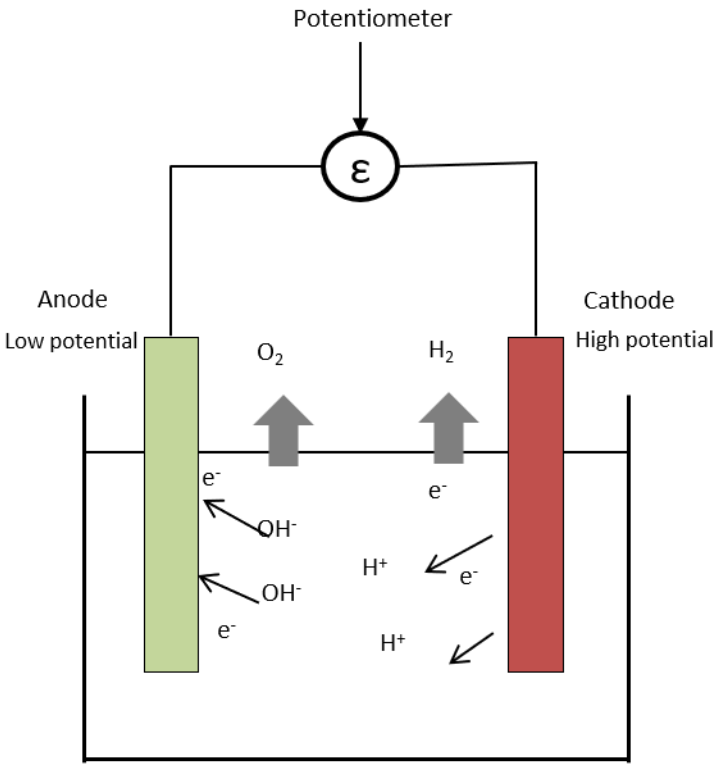

Figure 2-6 Potentiometer setup [13]

From this above equation, the pH value can be calculated, where the constant and β are calculated with the known solution. A pH electrode should be calibrated with two or more standard buffers before use. The pH of the unknown solution should lie within the range of the standard buffers.

2.3.2 COULOMETRY

In coulometric measurements the quantity of electric charge passes through the analyte during the electrochemical reaction is recorded. Faradays law of electrolysis explains that the current flow for a specific time through an analyte provides the total charge consumed by the solution. The charge of the electron is $1.69e^{-9}$, hence the charge in one mole ($6.022e^{23}$) of solution would be 96,485C. Thus, the quantity of electricity needed to complete the electrolysis determines the amount of analyte present in the solution. The general application of coulometry is identifying the rates of the ion transfer in the analyte.

2.3.3 VOLTAMMETRY

Voltammetry controls the electrode potential and measures the resultant current. The ionic movement depends on three principle convection, migration, and diffusion. In convection, the particles move in the solution based on the stirring. Migration happens due to the attraction of the electric field. Diffusion is due to the concentration gradient of the chemical compounds present in the analyte. The movement of the particles based on the principle is utilized in Voltammetry. Voltammetry uses pulse, linear and cyclic excitations based on how the reaction needs to be controlled in the cell and so the

techniques are named as stair case, rapid scan, and cyclic voltammetry. The goal is to record the peak currents in the solution at these excitations.

In voltammetry, the potential of the working electrode with respect to the reference electrode is varied at a steady rate on both sides of the equilibrium potential. This generates a current in the counter electrode. The difference between E and E° determines the cathodic (if E - E° is negative) or anodic current (if E - E° is positive) and thus reduction or oxidation of the analyte is determined. When an eternal voltage v is applied then at any given time the total potential is given by,

$$E(\mathrm{t}) = \mathrm{E_i} - \mathrm{v_t} \tag{2.13}$$

Where, Ei is the initial potential. Thus, the above equation becomes,

$$\mathrm{E_i} - \mathrm{v_t} - \mathrm{E}^{\circ} = 2.3\ \frac{\mathrm{RT}}{\mathrm{nF}} \log\left(\frac{\mathrm{M}^{+}}{\mathrm{M}}\right) \tag{2.14}$$

This curve shows the response of only the oxidized species on left of the origin and the reduced species in the right of the origin. When E - E° is positive the oxidation happens as it falls to zero volts the reduction of oxidized species will happen thus increasing the electron at the surface of the electrode. This will induce the diffusion between the bulk and the surface of the electrode, which attracts the oxidized species to the surface and pulls back the reduced species in the bulk. This will further increase the reduction current. The sweeping potential depends on the reference electrode.

The analysis on this paper is done for the pH measurement. In case of pH measurement, the ion concentration should not be disturbed. But in voltammetry the application by itself requires the chemical reaction, which disturbs the concentration of the solution. Thus, using ISE with potentiometric setup is the best method to measure the pH.

2.3.4 AMPEROMETRY

The electro chemical reaction happening in the electro chemical cell is based on the electron transfer happening on the surface of the working electrode also called the sensing electrode. So, the environment of the electrolyte is observed based on the working electrode, which should be polarized electrode. Which means there should not be any electron transfer due to the electrode and stays insensitive to the potential applied.

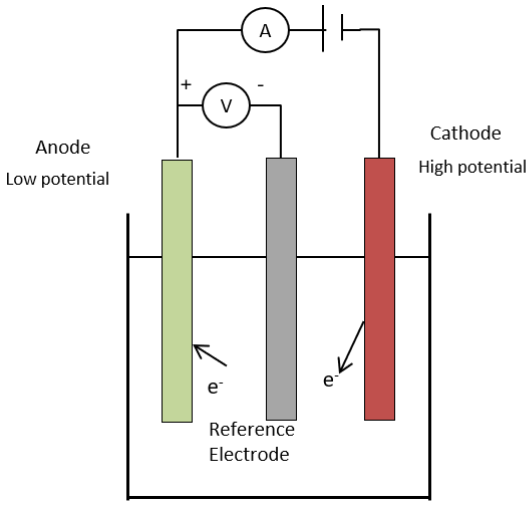

Figure 2-7 Amperometry with three electrode method [15]

The reference electrode on the other hand should be non-polarized and should able to supply a constant potential with minimum current flowing through it and should have a

dynamic equilibrium (reversibility). The WE and RE are sufficient for sensing application, but to meet the current requirements of the working electrode a third electrode can be used called counter electrode(CE). The operational amplifier dries the current between the WE and CE. This circuit is called potentiostat as shown in figure 2-7, care should be taken that the CE area is large to facilitate the current requirements.

The potential of the working electrode is varied with respect to the reference electrode based on the fermi level of the working species the current will vary based on the electrolytic reaction. The choice of the working electrode is very important as this can involve multiple species study.

The advantages are excellent sensitivity with a linear concentration rage for both organic and inorganic species. Rapid measurements can be done in seconds for multiple analytes.

The disadvantage of the cyclic voltammetry and amperometry are the current increases in response to the increasing potential but as the reduction happens, a diffusion layer is formed and the rate of the electrode reduction becomes diffusion limited. At this point the current slowly declines and results in an asymmetric peak-shaped I-E curve. The second disadvantage is the development of additional ohmic potential due to the internal resistance of the cell, which reduces the actual measurement.

The applications are quantitative determination of pharmaceutical compounds, metal ion concentration in water, determination of redox potential, determination of eluted analytes in High Performance Liquid Chromatography.

2.3.5 IMPEDANCE SPECTROSCOPY

The Electrochemical Impedance Spectroscopy provides more information than other static techniques or dynamic measurements. This method is capable of distinguishing between two or more electrochemical reactions taking place in the environment. Unlike amperometry it can identify diffusion-limited reactions and provide information on the capacitive behavior of the system. Electrochemical cells can be modeled as a network of passive electrical circuit elements. The response of the electrochemical cell recorded and an equivalent RLC circuit can be developed.

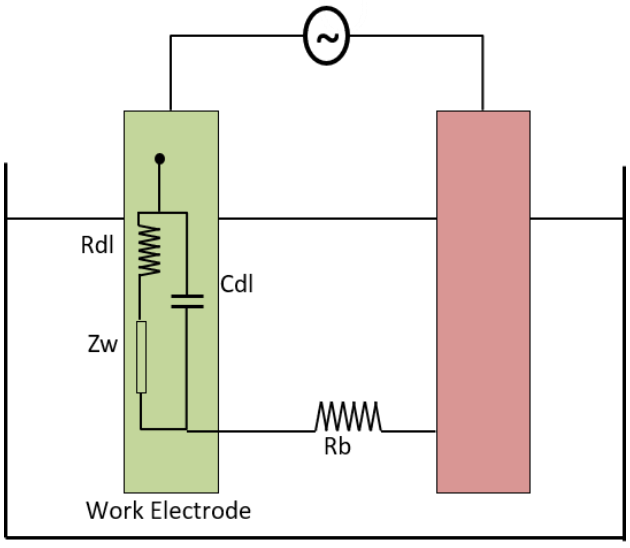

Figure 2-8 EIS setup with the bulk and double layer representation [14]

R_b is the electrolyte bulk resistance; C_{dl} and R_{dl} are the capacitance of the charge double layer. Z_w is Warburg Impedance. Warburg Impedance is the general impedance which

represents a resistance to mass transfer, i.e., diffusion control, typically exhibits a 45° phase shift at the lower frequencies.

The capacitance at the metal/electrolyte interface always plays an important role. The response of the system as a function of the perturbation frequency can reveal internal dynamics. Figure 2-8 shows the setup of the impedance spectroscopy. The advantages of this application are the availability of time dependent data, non-destructive and suitable for high resistance material like paints. But all these facilities come at a higher expense and complex data analysis.

The application of EIS can be done in engineering process as a characterization tool helps in surface optimization and quality control. This is used for protocol development for engineered surface topography and on-line process feedback.

2.4 pH SENSING READ OUT TRENDS

2.4.1 PH SENSING AND ION SELECTIVE ELECTRODE

The pH electrode operates in ion selective principle. The electrodes used for pH measurement method is called ion selective electrodes or glass electrodes. It has a thin glass membrane that is sensitive to hydrogen ions. To determine the hydrogen ion concentration, it uses potential difference between the reference electrode and measurement electrode. Diluted hydrochloric acid for example has large CL^- and small H+ ions. When pH sensor is immersed in the HCL liquid the H+ ions penetrate the boundary of the glass electrode also called gel layer. Where the CL^- ions remain in the solution the result is the charge separation. The same process happens on the inside of

the glass electrode where it has the buffered solution that has a pH of 7. The hydrogen ion concentration remains constant for the buffered solution that is present inside the glass electrode. If the hydrogen ion concentration on the inside of the glass electrode differs from the concentration of outside the glass electrode then a potential difference is formed. This potential difference is used to determine the pH of the solution.

The hydrogen ions present in the solution determine the pH of a solution. The acidic nature of the solution is proportional to the amount of hydrogen atoms present. The more the number of hydrogen ions the less the pH is depicted in figure 2-9. A solution with a pH of 7 is neutral which has 10^7 hydrogen atoms. The pH electrode works by ion exchange principle. When the electrode is dipped in the test solution the ions moves towards the glass surface and replace the metal ions. This changes the hydrogen ions movement on the surface of the electrode and accordingly the potential built across the electrode is affected. As stated in the above section potentiometric method is best suited for the pH measurement. There are several factors to account for during the pH measurement of a test solution.

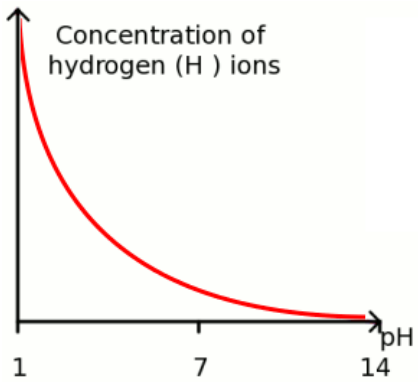

Figure 2-9 Hydrogen ions vs pH concentration

Temperature and sensitivity affects precision of potentiometer. This makes the reproducibility poorer. The sensitivity is determined by RT/nF in the Nernst equation. The better the ‘n’ i.e. the number of electrons involved in the redox reaction the sensitivity is good. The selectivity coefficient of the ISE is important; this determines that the electrode can be used for the sample. In real time application, the usage of the ISE plays an important role. The repeated usage limits the ISE sensors life time, though rinsing the electrodes between the samples keeps the sensor alive for a while.

2.4.2 MOSFET AS pH SENSOR AND OPERATION

The pH sensing performed with non-glass sensor is based on Ion Selective Field Effect Transistors. They use a MOS transistor arrangement; here the gate oxide acts a selective membrane for the test solution. MOSFET sensors convert the pH concentration on the solution into electrical signals such as voltage. This electrical signal is then converted to digital with analog to digital convertors. Thus it is very important the readout circuit is accurate and at the same time produces less noise and consumes less power. Figure 0-2 is the equivalent model of the FET sensor, and is very important to understand the operation. In a FET sensor the reference electrode is the gate of the FET, which is separated from the silicon dioxide.

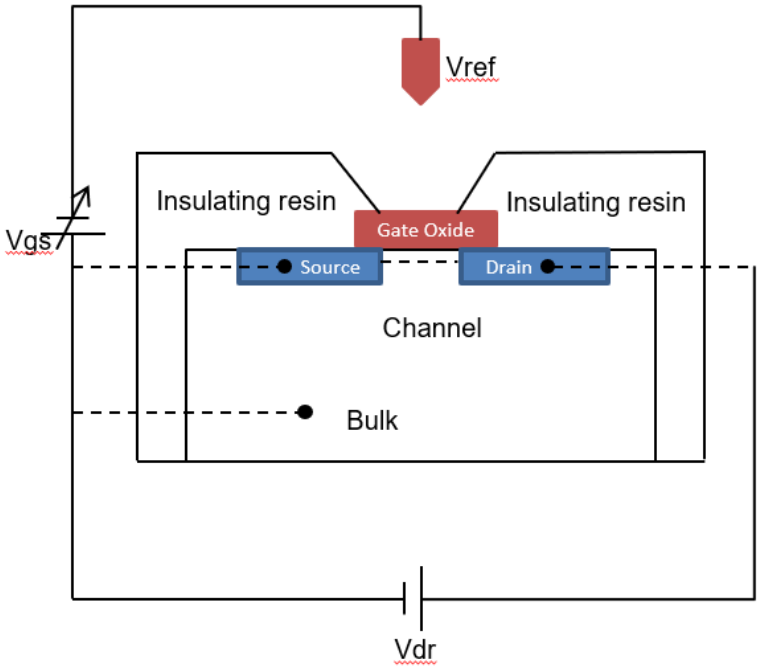

Figure 0-3 ISFET structure [16]

Thus, the change in pH will change the oxide potential which is described by extended site dissociation model [16].

Higher the H+ ions lower the pH value and vice versa. This change in the concentration of the ions changes the Vt of the FET. Now if the Vt increases the inversion layer starts to disappear and to overcome this the V_g must be increased. As the V_g is connected to the reference electrode, the potential of the reference electrode must be modified. In case of Vt decreases due to the decrease in the H+ ion concentration. There are other materials used as a dielectric in the FET like Al_2O_3 and Si_3N_4 for better pH sensitivity and selectivity. FET sensor needs a constant drain current for its operation, so that it changes the source to drain current with respect to the pH change. Apart from the selectivity and sensitivity the other factors to be considered for the sensor is hysteresis and drift.

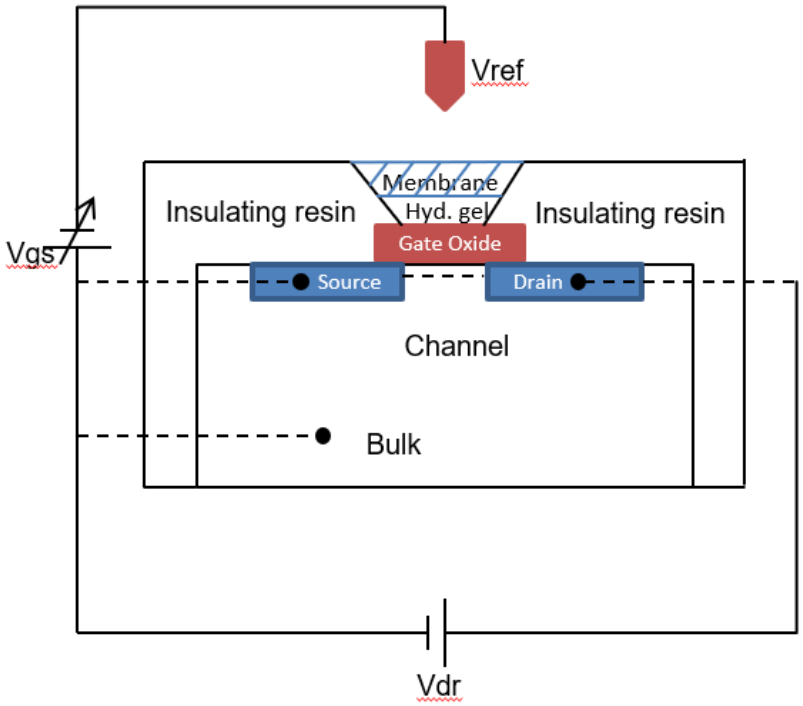

Figure 2-11 CHEMFET structure [16]

The reference electrode to be chosen plays an important role. For example, the calomel electrode has a TC of 0.8mV/ ºC for a saturated solution. The electrolytic solution also shows changes in dissociation with respect to the temperature. This in turn affects the pH measurement.

If the gate oxide is covered with ion-sensitive membrane then it is called MEMFET. MEMFET can be modified chemically to provide better thermodynamic interface at the gate which is called as CHEMFET as in Figure 2-11. The presence of CO_2 in the aqueous solution causes the thermodynamic instability, which penetrates the gate oxide. To avoid this hydrogen gel layer is introduced between the ion selective membrane and

the gate oxide. The readout circuit in this application is designed for sensor specification mentioned in table 2-1.

Table 3-1 Sensor specifications

Parameter	**Value**
Sensitivity	50mV/pH
Range	pH1- pH12
Response Time	10s
Biased Ids, Vds	25uA, 0.3mV
Output Voltage	+/-1.5V
Sensitivity material	Si_3N_4

2.4.3 READ-OUT CIRCUITS

The initial design for potentiometric sensing started with the conventional differential amplifier as in *Figure 2-12*. As sensors used for sensing pH and potentiometric sensing use the same electrochemical principle similar electronic interfacing circuits are used. In case of a MOSFET sensor the potentiometric readout circuit would detect the change in the pH across the source and drain of the sensor. The general challenges in MOSFET sensor are trapped charges, drift, capacitive attenuation, and temperature effect and noise corruption. FET sensor can operate in two different regions, saturation and inversion region. In the week inversion region, the current follows the exponential change

in the gate source voltage and in the saturation region the current follows the square law. In this section the trends used in pH sensing are discussed based on the region of operation of the MOSFET sensor. The measurement of the sensor can be carried out in two different ways, either varying the V_{ref} of the reference electrode or the threshold voltage (V_t) of the FET sensor with respect to the pH. The first method is not reliable as it changes the biasing conditions of the circuit and leads to complexity. The second method is globally used and there are two techniques to maintain the current.

- Source and drain follower or Constant Voltage, Constant Current (CVCC). In this method, the current Id and drain voltage V_{ds} are fixed, and the source voltage V_s is changed with respect to the pH. The advantage of this technique is it occupies lesser area and the design is immune to the capacitive scaling.
- Current mode read out method is the widely-used method where the MOSFET sensor is operated in weak inversion mode and the drain to source current (I_{ds}) are measured. This method requires current feedback read out and larger transistors are required, which increases the area and power consumption of the readout circuit.

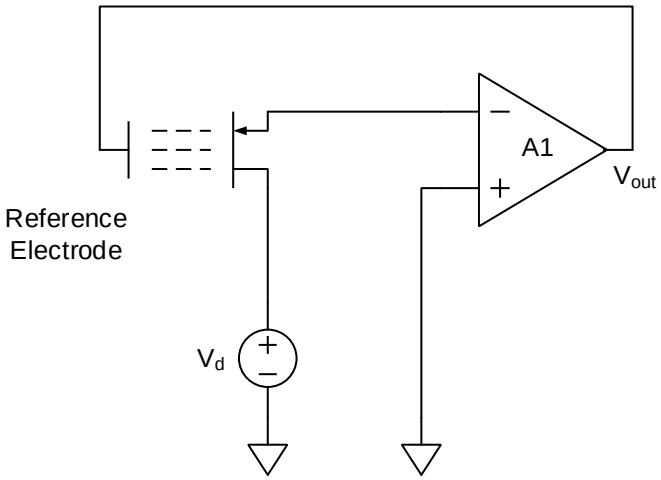

Figure 2-12 ISFET sensor readout circuit. [31]

Figure 2-12 shows one of the earlier techniques used to measure the pH. The reference potential at the electrode is maintained at a constant value. The potential at the source is the same due to the feedback. Considering the voltage at the source as V_s, varying the current I_{d1} and I_{d2}, the change in the output voltage for the pH value remains the same.

The general architecture implemented for the measurement of pH using ISFET is the differential topology. This provides the option to eliminate the temperature dependency and the drift using MOSFET. For this REFET sensor, which is a variation of ISFET, is used with known temperature characteristics. Also, the electrical characteristics of RFET sensor should match the CHEMFET sensor. This diode is fabricated adjacent to the CHEMFET for faster response and to provide accurate temperature compensation.

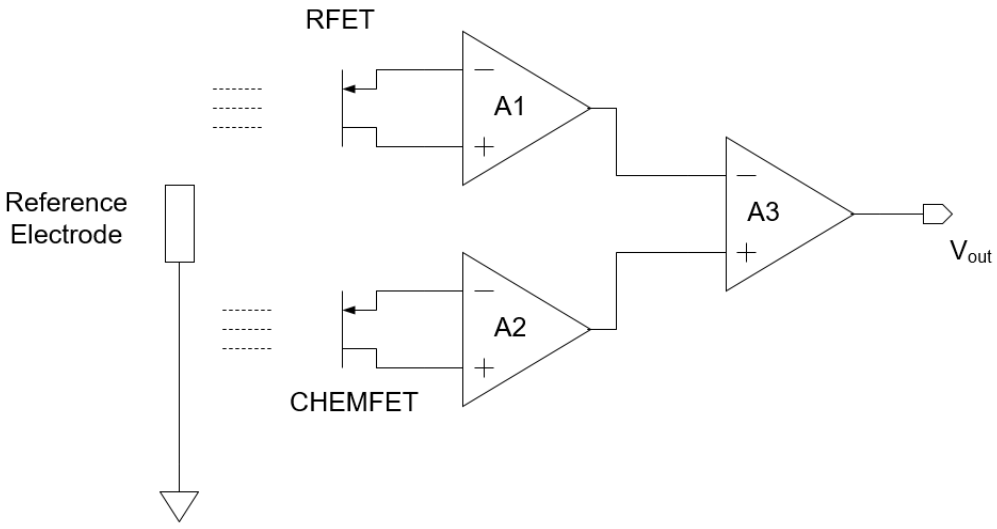

Figure 2-13 ISFET sensor readout circuit using differential amplifier. [47]

Figure 2-13 is the implementation of the RFET and CHEMFET sensor readout circuits. The V_t of the sensor is measured with the reference electrode grounded, otherwise called as the gate of the sensor in this application. But even with this architecture the noise in the measurement would dominate and hard to achieve the accurate potential at the output.

Summary of different architectures is presented below.

- All the architectures are based on OPAMP and thus do not take full advantage of integration.
- Architectures are complex and not compact.
- Architectures are power hungry and generate larger noise.
- Reference voltage needs to be generated externally or internally.

- As a result, these circuit architectures are not suitable for portable applications.

Potentiometric signal generated by the CHEMFET is of very low frequency. At low frequency, flicker noise is dominant. This is caused by the traps in the oxide of the MOS. It is purely dependent on the process and non-deterministic. The noise may destroy the actual signal, thus the amplifier used should have low input referred noise.

The disadvantage of existing architecture is larger power consumption and noise which is a down fall for portable applications. In real time environment for an in-vivo application area, noise and power are the important factors. Technology nodes limit the area. But noise and power are the two factors which always require improvement. Without compromising the performance parameters like gain and op-swing it is a challenge to improve the noise and power. Also, there is trade-off between noise and power which needs to be balanced. CMOS amplifiers usage is limited by the non-deterministic noise like flicker, short and thermal. The external filter circuit like RLC can reduce the noise though the power consumption is too high.

Where C is the load capacitance, n is the noise factor i.e. $1+A_v$, K is bolts man constant and T is the temperature, A_v is the gain of the amplifier. 1/f noise and the thermal noise are the most dominant noise factors in the op-amps. For low frequency applications 1/f noise is dominant and for wide band application white noise is dominant. Noise can be filtered by increasing the capacitance, but this would increase the power. As mentioned in the previous section the potentiometric sensing is done at lower frequency. Thus, eliminating flicker noise is the challenge in the design.

This leads to find the compensation techniques such as correlated double sampling which helps avoid drifts and offset, which proves to improve the noise performance and power consumption.

CHAPTER3

3.1 PROPOSED CMOS CDS WITH SWITCHED CAPACITOR LP FILTER

CMOS technology shows very accurate, stable results with temperature change, easy offset correction factors, rail to rail outputs, and low power consumption with linear voltage change. These features make CMOS as the most desired technology node. Correlated double samplers are very useful in the process of digitizing the sensor outputs with reduces noise and offset. A less-obvious consequence for the amplifier's operation is the low-frequency "1/f noise" characteristic. In "normal" amplifiers, the input voltage noise spectral density increases exponentially inversely with frequency below a "corner" frequency, which may be anywhere from a few Hz to several hundred Hz.

3.1.1 CORRELATED DOUBLE SAMPLING CIRCUIT

Potentiometric sensors that are used for pH measurement in this application operate at a lower frequency. The signal generated by the sensor can be sampled in the capacitor and can be amplified accordingly with the help of the op-amp used in the section 3.2.1. One such architecture is discussed in Figure 3-1, otherwise called correlated double sampler. With the help of the non-overlapping clocks, $\Phi 1$ and $\Phi 2$, the signal can be sampled and stored at the output capacitor. This technique effectively reduces the 1/f noise. It helps to enhance the gain of the circuit and is used in sampled circuits, where the noise behavior is not made worse by aliasing.

3.1.2 NOISE SOURCES AND CORRELATED DOUBLE SAMPLING

Thermal and flicker noise are the dominant noises present in modern electronics. In MOS transistors thermal noise is created by the drain current fluctuation. The random motion of the charge carriers produces thermal noise given by equation 3.1.

$$S_1 = \frac{2KT}{Ron}\ [A^2/Hz] \tag{3.1}$$

Where, k is the Boltzmann constant k, $1.38*10^{-23}$ J/K, T is absolute temperature of the device in degrees Kelvin, and Ron is the on-resistance in ohms for the transistor.

Flicker noise which is also called as 1/f noise caused by the trapping of the charges during their movement from source to drain of the transistor. The flicker noise power spectral density is given by the equation 3.2.

$$S_f = \alpha * \frac{I}{f.N}\ [A^2/Hz] \tag{3.2}$$

Where, α is Hooge's factor from the Hooge's bulk mobility fluctuation model, f is the frequency of operation and N is the number of carriers. The 1/f noise increases with the decrease in the number of carriers and would be a bigger issue with the reduction in technology node.

Figure 3-1 shows the operation of correlated double sampler circuit. Clock $\Phi 2$ is high the switch S1 helps to transfer the charge stored in the capacitor C_1 to the Capacitor C_2. The amplifier allows the charge to be transferred to the second stage without loading. When clock $\Phi 2$ is high the switch S2 helps the capacitor C_2 to discharge and get it ready for the next sample transfer, while the capacitor C_1 is charging.

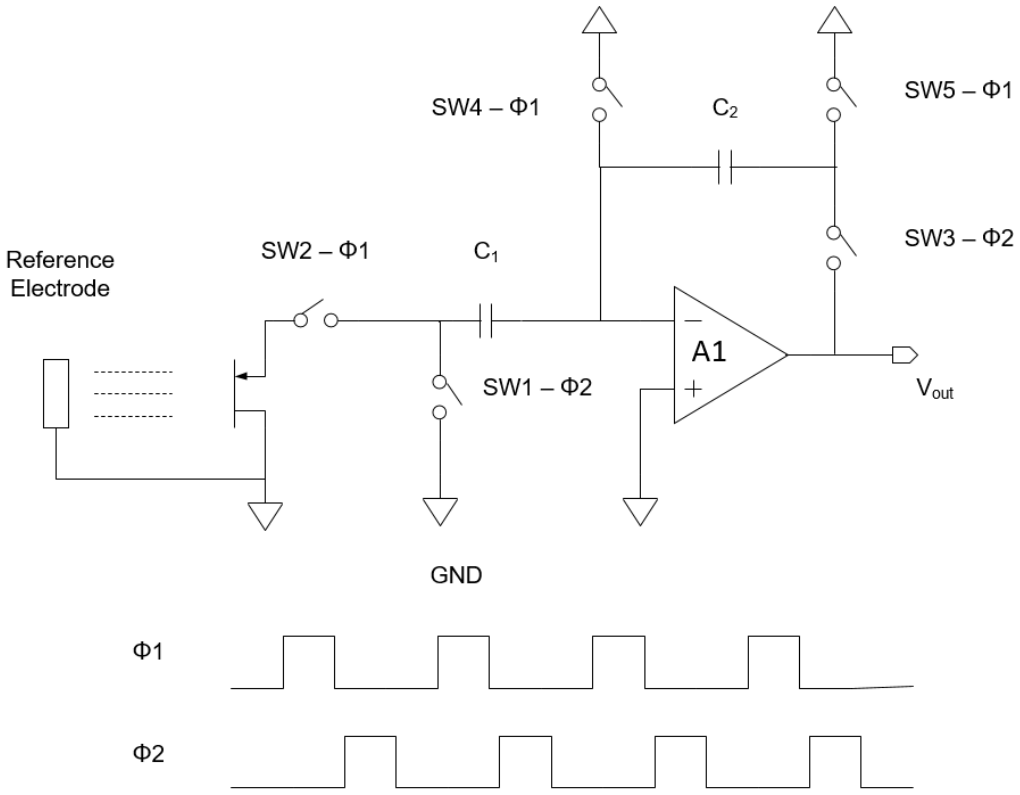

Figure 3-1: Correlated double sampler circuit [47]

The feedback network and the input resistors are designed with a resistor emulator instead of a passive resistor. The resistor emulator operates with clock frequency of 1MHz. Here the data is not present for a continuous time period and so as the noise generated by the circuit is also not continuous. Thus, we can control the voltage stored in the capacitor by varying the ON time of the switch. In this design the series switch SW1,

SW2, SW3, SW4 and SW5 in Figure 3-1 is implemented using a transmission gate. This reduces the overall noise of the system, which is explained as follows.

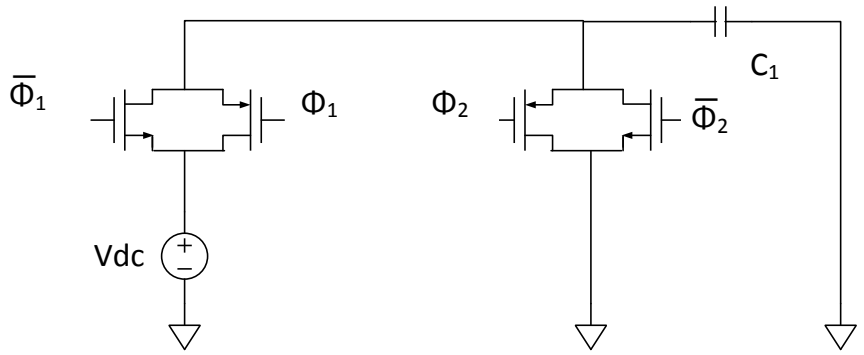

Figure 3-2: Implementation of the resistor emulator for sampling stage.

In the correlated double sampler shown in figure 3-1 two-stage op-amp implementation along with the switch cap can be modeled as shown in the section 3.2.1. For the CDS the switch and the capacitor are modeled with the noise source. The ON resistance of the switch is 10mOhm and the capacitor C1 that is shown in figure 3-2 can sample the input signal and the noise.

The switching frequency of the switch SW2 in figure 3-1 is decided by the ON time of the clock Φ1, the capacitor C_1. Thus, the time constant of the switch is a factor of sampling capacitance C_1 with the ON resistance of the switch added to the input impedance of the op-amp.

The closed loop gain of the amplifier A1 in Figure 3-2 is $G = (1+C_1/C_2)$ and the 1st pole frequency would be $\beta g_{mn6}/C_c$. Where C_c is the compensation capacitor used in op-amp design. The operation of the switch capacitor on the designed amplifier is decided by two

steps sampling and Integration. Here R_{on1} of the switch is represented as R_{on} and noise is represented as V_{Ron1} similarly R_{on2} of the switch is represented as R_{on} and corresponding noise is V_{Ron2}. At sampling stage, the total noise power is defined as,

$$V_{c1}{}^2 = V_{c1,op}{}^2 + V_{c1,sw1}{}^2 + V_{c1,sw2}{}^2 \tag{3.3}$$

Here sw1 and sw2 are the switches corresponding to R_{on1} and R_{on2}.Also, Only C_1 is considered as that is the limit for the sampling and the noise generated by C_1 will be transferred to the output. Thus, producing the total noise of,

$$V_{c1}{}^2 = 2 * \frac{\gamma KT}{C_1} + \frac{KT}{C_1} + \frac{KT}{C_1} = \frac{2KT}{C_1}(\gamma + 1) \tag{3.4}$$

The spectral density is given by integrating the noise over the frequency,

$$S_{nc1}(f) = \int_{-\infty}^{\infty} \frac{2KT}{C_1}(\gamma + 1) \left| H(j2\pi f) \right|^2 df \tag{3.5}$$

Where, f_{eff} is the effective noise bandwidth or the cutoff frequency of the RC circuit, integrating f_{eff} over the frequency spectrum here gives the equation (3.6).

$$S_{nc1}(f) = \frac{2KT\gamma}{C_1}(f_{eff}) = \frac{2KT\gamma}{C_1 . 4\tau} \tag{3.6}$$

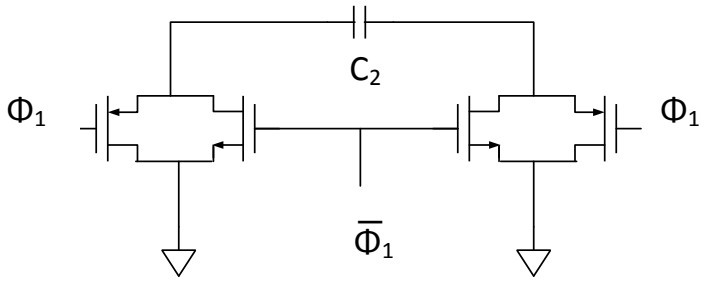

Figure 3-3: Implementation of the resistor emulator for the feedback.

From equation 3.6 it can be see that the total noise that is stored in the capacitor over the bandwidth of the CDS circuit is S_{nc1}.

The values of the capacitors in the resistor emulators used in Figure 3-2 and Figure 3-3 are chosen based on the charge transfer rate which is the switching frequency of the resistor emulator. If V_{in} is the voltage sampled at the sensor input, then the charge stored in the capacitor is given by $C_{1*}V_{in.}$ The charge transfer is happening at a switching frequency f, and then the rate transfer charge per unit time at the input is given by equation 3.7,

$$I_{in} = q_{in} * f \tag{3.7}$$

$$R_{in} = \frac{V_{in}}{I_{in}} = \frac{1}{C_1 * f} \tag{3.8}$$

Thus, from the equation 3.8 for any value of resistor chosen the value of C_1 is can be chosen. In general, the switching frequency is chosen as the cutoff frequency of the correlated double sampler. A similar procedure is used to choose C_2 shown in figure 3-2. Now as the noise integrated by the capacitor C1 is given by S_{nc1} as in equation 3.6 switching the charge rate of the cap C1 at a higher rate than the cutoff frequency of the correlated double sampler will help reducing the noise.

Thus, implementing the resistor emulator with switch SW1 and SW2 with a capacitor C_1 over a closed loop op-amp will reduce the noise produced by the designed op-amp. For this design the sampling time used is 20ns with a capacitor value of 100nF and length of the input transistor NM6 is 1μm.

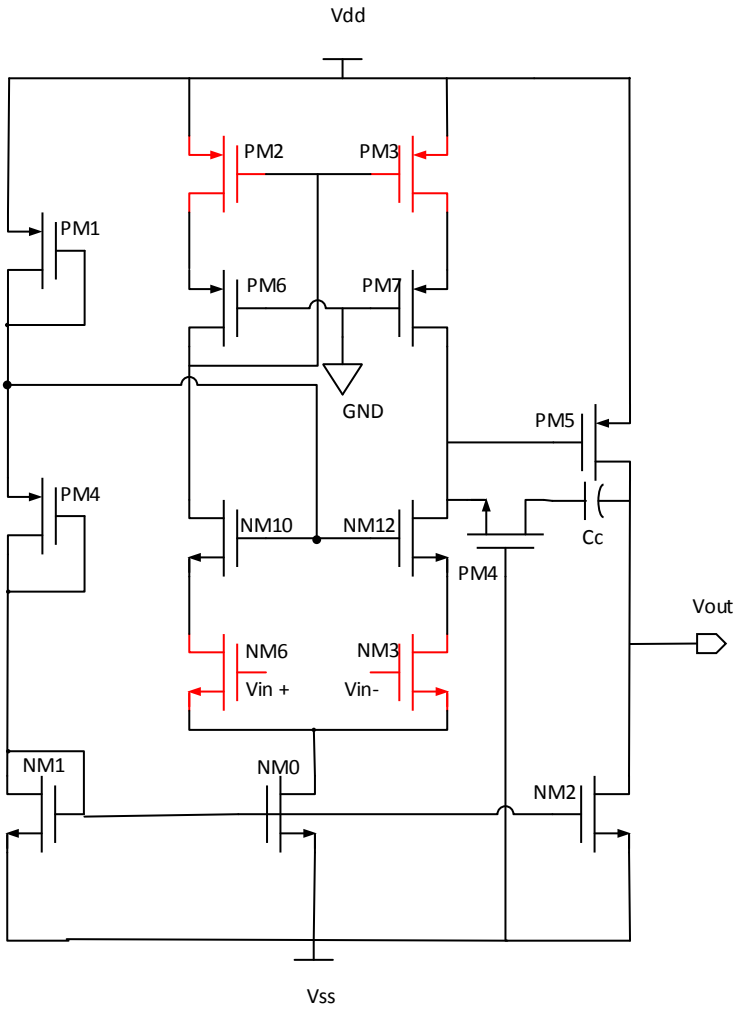

Figure 3-4: Transistors that are critical for noise in the architecture.

The highlighted transistors in the in the figure 3-4 NM6, NM5 and PM2, PM3 are the major noise contributors in the circuit as these transistors are present in the signal path.

As the potentiometric application works at lower frequency the dominant noise in this region of operation is flicker noise. The flicker noise of an op-amp is given by the equation 3.9 shows that the noise increases as the frequency decreases.

$$S_{nflicker}(\mathrm{f}) = \frac{2K_f}{C_{ox} \cdot W_{n6} \cdot f}\left[\frac{1}{\mathrm{L}_{n6}} + \frac{\mathrm{K}_{p6} \cdot \mu_{p6} \cdot \mathrm{L}_{n6}}{\mathrm{K}_{n6} \cdot \mu_{n6} \cdot {\mathrm{L}_{p6}}^2}\right] \quad (3.9)$$

Here, the noise is derived from both the input transistor NM6 and the load transistor PM6. Where K_{p6}, µp6 and L_{p6} are the relative permittivity, mobility and length of the PMOS transistor used and K_{n6}, μ_{n6} and L_{n6} are the relative permittivity, mobility and length of the NMOS transistor used.

Equation (3.9) defines the minimum noise that the closed loop op-amp can produce. Thus, it proves that noise can be minimized by increasing the W/L ratio of the transistors NM6 and PM6. This is discussed in section 3.2.1 op-amp analysis. To reduce noise the switches must operate in a frequency that these flicker noise can be reduced. The flicker noise equation shows that the dominant noise is produced by the W/L size of the transistors NM6 and PM6. Thus, choosing W/L is very important the length of the channel is chosen as 1µm this would reduce the input referred noise. This would determine the dominant pole of the amplifier. As dominant pole of the amplifier set now the 3dB frequency can be determined. Once the cutoff frequency of the amplifier is determined the switching frequency of the clocks Φ1 and Φ2 can be determined using equation 3.10. Normally the switching frequency is set much higher than the 3dB frequency to achieve better noise performance, in this scenario the clocks of the switches are set to 1MHz.

3.1.3 CMOS CDS WITH CONVENTIONAL LP FILTER

The architecture in Figure 3-5 shows the CDS with a conventional low pass filter. Here V_{in}^2 is the input voltage noise of the CDS and V_{cds}^2 and V_{lp}^2 are the output noise of the

CDS and low pass filter. The first pole falls at the -3dB location (f1) of the gain, so that the transfer function $H_{cds}(f)$ of the system with the cutoff frequency f1 is given by equation 3.11. This is then passed to the low pass filter where the 3db pole is at f2, thus integrating the transfer function of the low pass filter $H_{lp}(f)$ with the noise generated by the previous stage would result in the over noise of the system.

The transfer function of the CDS is given by the equation (3.10) [1],

$$|H_{cds}(f)|^2 = \left| \frac{2}{\frac{0.3f_1}{f} + 1} \right|^2 \quad (3.10)$$

The equation (3.11) shows the low pass filter transfer function [1],

$$|H_{lp}(f)|^2 = \left| \frac{A_0}{\frac{jf}{f_2} + 1} \right|^2 \quad (3.11)$$

Here A_0 is the DC gain of the low pass filter and f_2 is the cutoff frequency of the low pass filter.

When clock $\Phi 1$ is high the switch S1 helps to transfer the charge stored in the capacitor C_1 to the Capacitor C_2. The amplifier allows the charge to be transferred to the second stage without loading. When clock $\Phi 2$ is high the switch S2 at the output of the first stage samples the data to the input of the low pass filter. Here the data at the output is continuous and noise of the transistors in the signal path of low pass filter circuit will be still appearing at the output. The figure 3.6 shows the equivalent model of the overall system, where the Cl at the input is the impedance of the correlated double sampler.

$$V^2cds = |H_{cds}(f)|^2 * V^2in = \left|\frac{2}{\frac{0.3f_1}{f}+1}\right|^2 * V^2in \quad (3.12)$$

The final noise generated V_{lp}^2 of the system is given by the equation (3.12) represents the total transfer function of CDS with LP filter system [1].

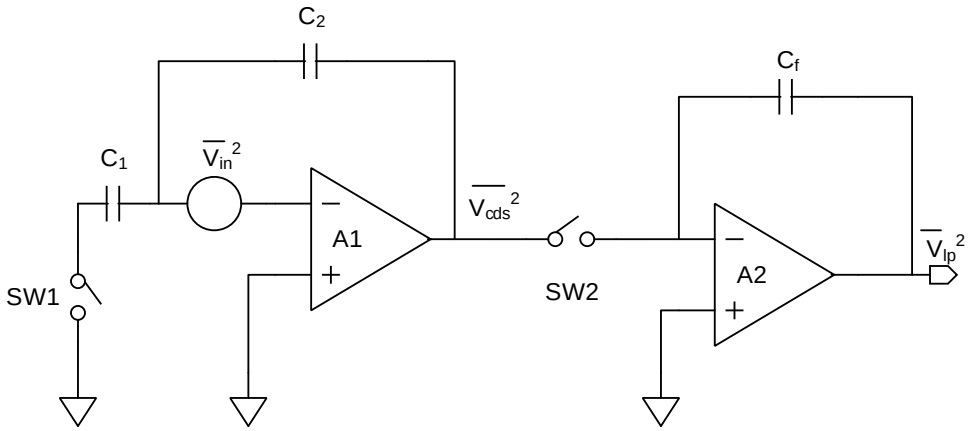

Figure 3-5: CDS with LP filter

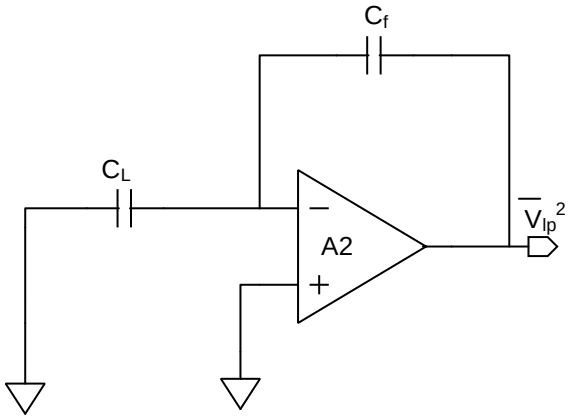

Figure 3-6: Equivalent model of Figure3-3 CDS with LP filter

$$V_{lp}{}^2 = |H_{lp}(f)|^2 \; V^2 cds = \int_0^{\infty} \left| \frac{A_0}{\frac{jf}{f_2} + 1} \right|^2 \left| \frac{2}{\frac{0.3f_1}{f} + 1} \right|^2 V^2_{in} \; . df \tag{3.12}$$

$$V_{lp}{}^2 = \left(\frac{C_l}{C_f}\right)^2 \frac{K_f}{C_{ox} WLf} \left(\frac{2\left(\frac{f}{0.3f_1 + f}\right)}{\sqrt{\left(1 + \left(\frac{f}{f_2}\right)^2\right)}} \right)^2 . df \tag{3.13}$$

Here, C_L is the impedance of the CDS; C_f is the feedback capacitor of the low pass filter, W and L are the width and length of the input transistor in the low pass filter, f is the unity gain frequency that is used in this design it is 20MHz. Here f_2 is the cut-off frequency of the low pass filter and f_1 is the frequency of interest i.e. the sensor output frequency, which is 100Hz. Equation (3.13), shows the noise generated by the closed loop system.

3.1.4 PROPOSED CMOS CDS WITH SWITCHED CAPACITOR LP FILTER

Focusing on reducing the noise further, generally the CDS is followed with a conventional low pass filter to maintain a high gain at the desired frequency. This would limit the noise reduction of the CDS stage. To overcome this limitation, a switch capacitor based low pass filter method can be used. As discussed in correlated double sampler section 3.1.1 the switching frequency and the resistor emulators are designed.

Figure 3-7 shows the novel CDS with switched capacitor based low pass filter. When clock Φ1 is high the switch SW1 helps to transfer the charge stored in the capacitor C_1 to

the Capacitor C_2. The amplifier allows the charge to be transferred to the second stage without loading.

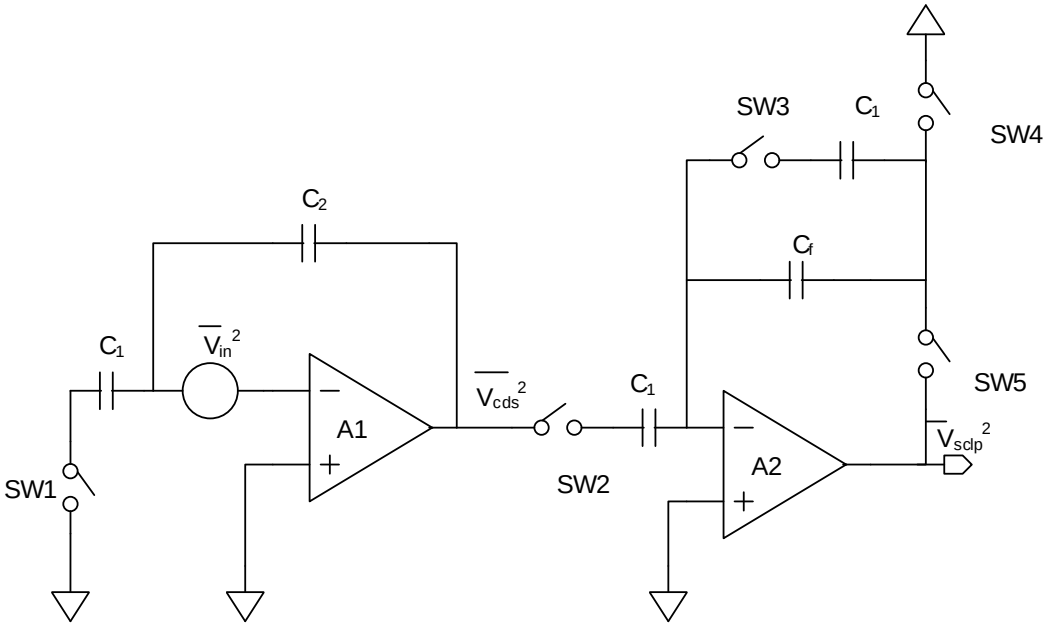

Figure 3-7: CDS with SCLP filter

When clock Φ2 is high the switch SW2 at the output of the first stage samples the data to the input of the low pass filter. The feedback network is designed with a resistor emulator instead of a passive resistor, which is in parallel with the filtering capacitor at the feedback. The resistor emulator operates with Φ1 clock. Here the data is not present for a continuous time period and so as the noise generated by the circuit is also not continuous. This reduces the overall noise of the system, which is explained as follows-

The transfer function of the CDS is given by equation 3.14 and the switched capacitor-based LP filter is given by the equation (3.15) [1],

$$|\mathrm{H}_{cds}(\mathrm{f})|^2 = \left|\frac{2}{\frac{0.3\mathrm{f}_1}{\mathrm{f}}+1}\right|^2 \tag{3.14}$$

Here $0.3f_1$ and f_2 are the 3db frequency of the CDS and the low pass filter. The 1/f noise of the CDS is given by,

$$\mathrm{V}_{cds\mathrm{f}}{}^2 = \mathrm{V}_{in}{}^2 . \frac{\mathrm{K}_f}{\mathrm{C}_{ox}\mathrm{WLf}} \; |\mathrm{H}_{cds}(\mathrm{f})|^2 . \mathrm{df} \tag{3.15}$$

Here $V_{in}{}^2$ is the input noise that is generated from the operational amplifier A1. When the LP filter is replaced with SCLP filter the transfer function modifies as shown in equation (3.16) which is derived with reference to equation (3.11) [1]. The switched capacitor based low pass filter's cutoff frequency is reduced by 0.3 times when compared to the conventional low pass filter. This helps in reducing the noise of the overall system further.

$$|\mathrm{H}_{sclp}(\mathrm{f})|^2 = \left|\frac{\mathrm{A}_0}{\frac{\mathrm{jf}}{0.3\mathrm{f}_2}+1}\right|^2 \tag{3.16}$$

The overall noise spectral density of the system is given by the product of the noise spectral density generated by the correlated double sampler and the switched capacitor based low pass filter,

$$\mathrm{V}_{sclp}{}^2 = |\mathrm{H}_{sclp}(\mathrm{f})|^2 \; \mathrm{V}_{cds\mathrm{f}}{}^2 \tag{3.17}$$

$$Vsclp^2 = \left(\frac{\mathrm{C}_l}{\mathrm{C}_f}\right)^2 \frac{\mathrm{K_f}}{\mathrm{C}_{ox}\mathrm{WLf}} \left(\frac{2\left(\frac{\mathrm{f}}{0.3\mathrm{f}_1+\mathrm{f}}\right)}{\sqrt{\left(1+\left(\frac{\mathrm{f}}{0.3\mathrm{f}_2}\right)^2\right)}}\right)^2 . \mathrm{df} \tag{3.18}$$

This clearly shows that the noise is reduced by a factor of 3.33 and the difference is shown in the noise spectrum density equation (3.18). Where, C_l totals capacitance seen by the second stage $C_l = C_2+C_1$. By integrating eq1 the total noise at the output of the LP filter can be derived as [1],

Where, f is the noise peak that can be inferred from the noise spectral density. Here C_f acts as the sampler and filter for the CDS system, this reduces the noise of the system compromising the BW of the system [2].

The f_1 of the CDS is chosen as 500Hz and the cutoff frequency of the LP filter is chosen as 1K. The above equation shows that choosing the peak noise frequency that will be seen at the output of the LP filter. Thus, from equation (3.18) by carefully choosing the LP filter feedback capacitor and 3db frequency of interest at the final stage the noise can be drastically reduced [1].

3.2 DESIGN SPECIFICATION

The proposed correlated double sampler with switched capacitor low pass filter design uses 0.18µm CMOS technology node. Table 3-1 is the design specification for the architecture used.

Table 3-1 Process specifications

Parameter	**Value**
VDD	+1.65V

VSS	-1.65V
Minimum L	0.35µm
PAD size	67µm*67µm
Resistance	7KΩ/square
Metal Layers	6

The device can operate at a power supply ±1.65V and the minimum channel length used is 0.35µm. There are six metal layers available in this technology to draw interconnects and 67µm*67µm is the bond pad size used on the QFN 208 pin package.

3.2.1 OP-AMP DESIGN & ANALYSIS

The operational amplifier used for the implementation of this architecture require a high gain in the first stage at the same instant it should be implemented for low power and low noise application. A cascade configuration based two stage OP-AMP will help this requirement. So, a CMOS telescopic amplifier is used. Since this op-amp is going to be used in switched capacitor based circuit, the limitation of the common mode input voltage in this topology can be ignored. Alternatively, it also consumes lesser power with the gain it can achieve.

The op-amp implementation for the correlated double sampler is shown in Figure 3-2. For the pH sensing application, the op-amp is configured with unity gain feedback and unity gain bandwidth of 20MHz. For pH the read-out is performed at DC. At DC the main noise source is 1/f noise and contributed by the two input transistors. During the design care should be taken so that the length of the NM6 transistor in the above Figure 3-8 is larger

than the PM6 and PM2 transistors. This will make sure the noise of the PMOS is not dominant. The noise density of the NM6 transistor is given by the equation (3.19),

The current noise generated by the input transistor NM6 is given by,

$$\mathrm{i}_{d6}{}^{2} = 4\mathrm{KT}\gamma \mathrm{g}_{mn6} + \frac{\mathrm{K}_{f}}{\mathrm{C}_{ox}\mathrm{W}_{n6}.\mathrm{L}_{n6}} . \frac{1}{\mathrm{f}} . g_{mn6}{}^{2} \tag{3.19}$$

Where, γ is 2/3, K_f is the flicker noise coefficient, C_{ox} – oxide capacitance, W and L are the width and the length of the transistor, g_{m6} is the trans conductance of the transistor. The corresponding voltage noise is given by,

$$\mathrm{V}_{nop}(\mathrm{f}) = \frac{\mathrm{v}_{d6}{}^{2}}{\Delta \mathrm{f}} = \frac{4\mathrm{KT}\gamma}{\mathrm{g}_{mn6}} + \frac{\mathrm{K}_{f}}{\mathrm{C}_{ox}\mathrm{W}_{n6}.\mathrm{L}_{n6}} . \frac{1}{\mathrm{f}} \tag{3.20}$$

For the op-amp design the first stage has NM6 as the input transistor and PM6 as the load which give the noise voltage in the path as shown in equation (3.21).

Also, $g_{mn6} = g_{mn3}$ so,

$$\mathrm{Sn1}(\mathrm{f}) = \frac{8KT\gamma}{g_{mn6}} + \frac{8\mathrm{KT}\gamma \mathrm{g}_{\mathrm{mp6}}}{g_{mn6}{}^{2}} + \frac{2\mathrm{K}_{f}}{\mathrm{C}_{ox}.\mathrm{W}_{n6}.\mathrm{L}_{n6}.\mathrm{f}} + \frac{2\mathrm{K}_{f}\, \mathrm{g}_{mp6}}{\mathrm{C}_{ox}.\mathrm{f}.g_{mn6}{}^{2}} \tag{3.21}$$

Here, $\mathrm{Sn1}$ is the total noise of the system that is including the thermal noise and the flicker noise. As, it could be see that the thermal noise parameters are independent of frequency and the flicker noise parameter shows that the increase in noise with decrease in frequency.

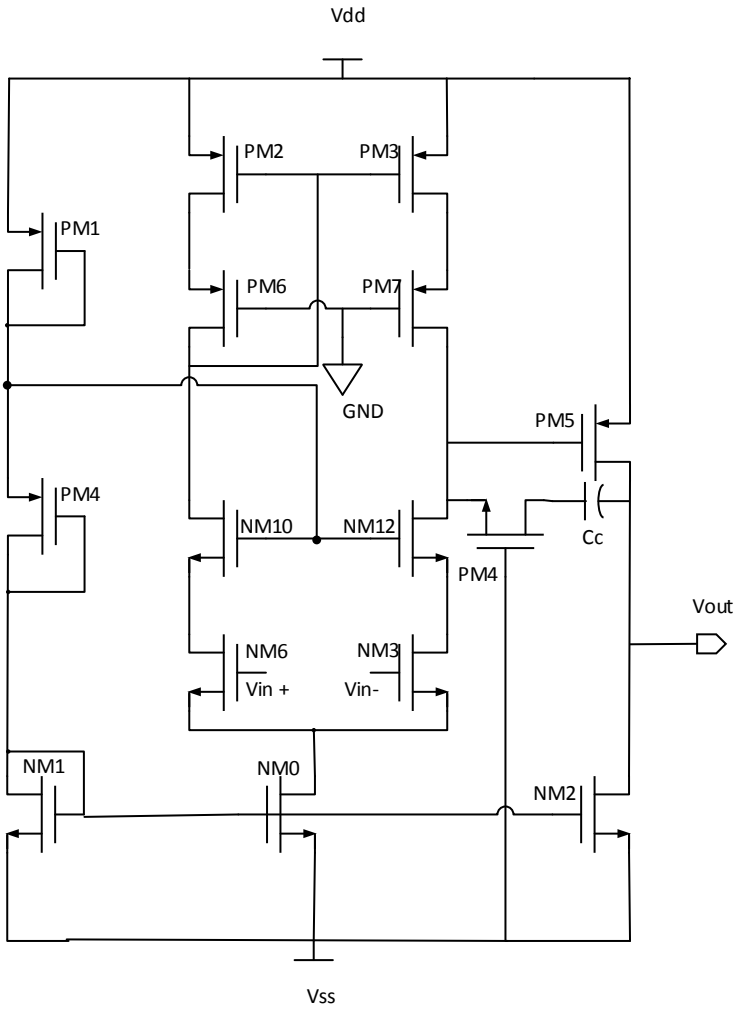

Figure 3-8: OP-AMP 1st Stage Telescopic architecture

With the second stage added the total noise of the circuit would be,

$$S_{ntotal}(f) = \frac{8KT\gamma}{g_{mn6}} + \frac{8KT\gamma g_{mp6}}{g_{mn6}^{2}} + \frac{2K_f}{C_{ox}.W_{n6}.L_{n6}.f} + \frac{2K_f\, g_{mp6}}{C_{ox}.f.g_{mn6}^{2}} + \frac{2K_f\, g_{mp9}}{C_{ox}.f.g_{mn6}^{2}} \quad (3.22)$$

Simplifying the equation (3.22) we get,

$$S_{ntotal}(f) = \frac{8KT\gamma}{g_{mn6}}[1 + \frac{g_{mn6}}{g_{mn6}}] + \frac{2K_f}{C_{ox}.W_{n6}.f}[\frac{1}{L_{n6}} + \frac{g_{mn6}}{g_{mn6}^2} + \frac{g_{mp9}}{g_{mn6}^2}] \quad (3.23)$$

At lower frequencies the flicker noise dominates the white noise thus the equation (3.23) can be simplified to,

$$S_{nflicker}(f) = \frac{2K_f}{C_{ox}.W_{n6}.f}[\frac{1}{L_{n6}} + \frac{g_{mp6}}{g_{mn6}^2} + \frac{g_{mp9}}{g_{mn6}^2}] \quad (3.24)$$

The noise over the frequency (Δf) were by assuming the width of the transistors are all the same. Noise Power spectral density of the two-stage op-amp is given by equation (3.25),

$$S_{nflicker}(f) = \frac{2Kf}{Cox.Wn6.f}[\frac{1}{Ln6} + \frac{Kp6\,.\,\mu p6\,.\,Ln6}{Kn6\,.\,\mu n6\,.\,Lp6^2} + \frac{Ln6}{Lp9^2}] \quad (3.25)$$

The potentiometric circuit's 1/f noise of closed loop op-amp can thus be derived as in equation (3.26),

$$Vnflicker^2 = \left(\frac{Rf}{Rin}\right)^2 \frac{2Kf}{Cox.Wn6.f}[\frac{1}{Ln6} + \frac{Kp6\,.\,\mu p6\,.\,Ln6}{Kn6\,.\,\mu n6\,.\,Lp6^2}] \quad (3.26)$$

In the equation (3.26) p6 and n6 are the input transistors of the amplifier as shown in figure 3-6. Rf is the feedback resistor and Rin are the input resistor, that determines the closed loop gain of the final stage of the amplifier. The noise spectral density purely depends on the transistor size, which is limited to the technology node.

The designed op-amp achieves an open loop gain of 110dB, unity gain band width of 20MHz, phase margin of 52º and consumes power of 44µW from 3.3V supply. Figure 3-9 shows the frequency response of the designed op-amp with the load capacitance of 1pF.

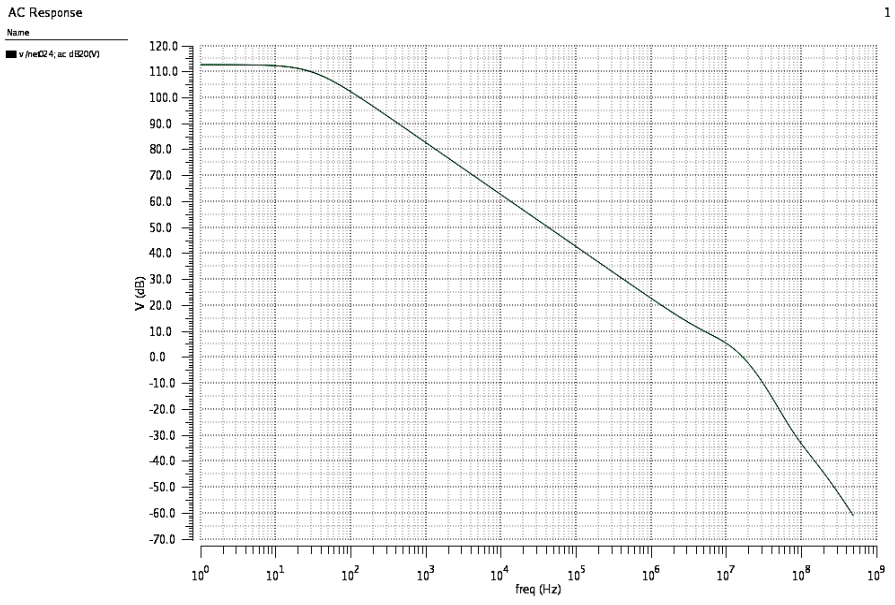

Figure 3-9: AC response of OPAMP gain (db) vs frequency (Hz).

The DC response of the designed op-amp is captured in Figure 3-10. To measure the swing the op-amp is connected in unity gain mode by shorting the inverting terminal with output and sweeping the voltage at the non-inverting terminal from ±1.5V. It achieves an output swing of -1.5V to +1.5V, this meets our CHEM resistor's requirement.

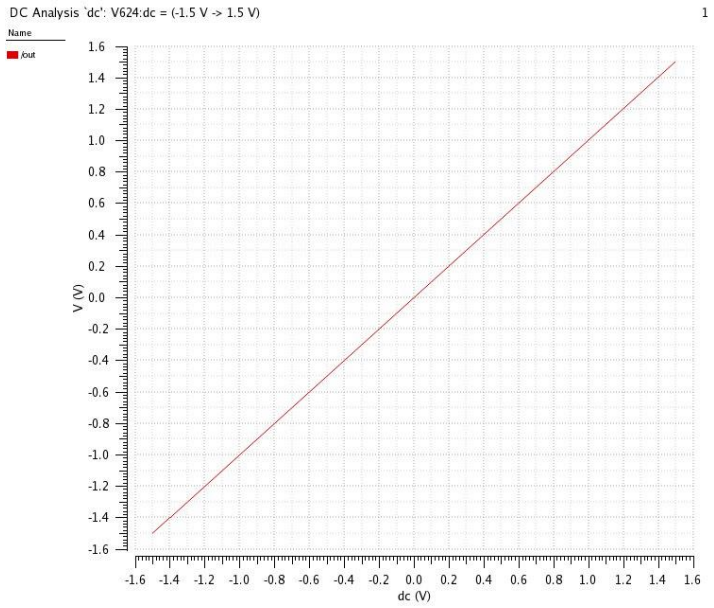

Figure 3-10: DC response of OPAMP Vin vs Vout.

To measure the noise of the op-amp, all the AC input voltages are set to ground potential and the RMS noise is measured at the output of op-amp. Integrating the noise over the frequency range of 1Hz to 20MHz is illustrated in Figure 3-11; the RMS output noise of op-amp is calculated to be 233µVrms.

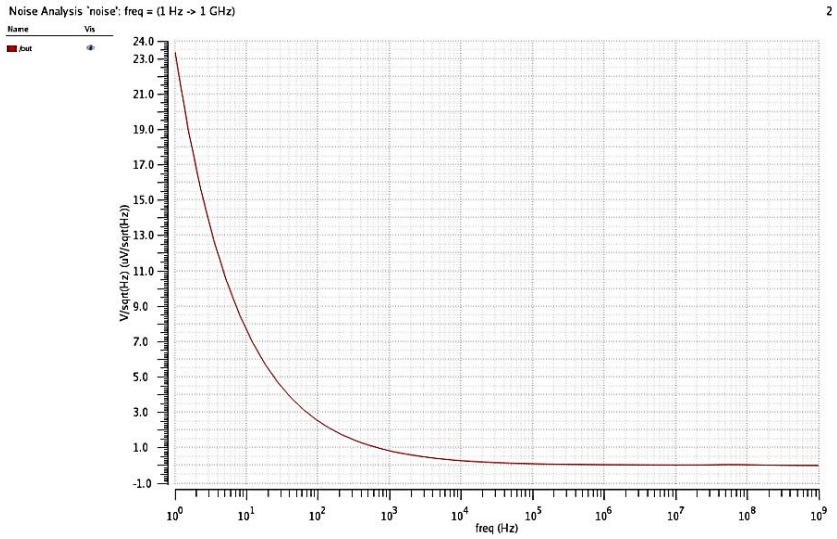

Figure 3-11: Noise analysis of OPAMP noise (µVrms) vs frequency (Hz).

3.3 SIMULATION RESULTS

The post layout is simulated with 1MHz clock frequency. The sampling capacitors with 100nF at 1Mz clock are used, with a load capacitor of 5nF. The input range used is from +1.5V to -1.5V obtained from the pH sensor specification.

3.3.1 CMOS IC LAYOUT OF PROPOSED CIRCUIT

The proposed architecture of the circuit is fabricated in 0.18µm CMOS technology node. Cadence tool is used to design the schematics and layout. The design rule check, post layout parasitic RC extraction is performed using Assura. The dimension of the designed chip is 990µm x 216µm. Figure 3-12 shows the proposed architecture

implemented in the system. The correlated double sampler with switched capacitor low pass filter is highlighted in yellow in Figure 3-12.

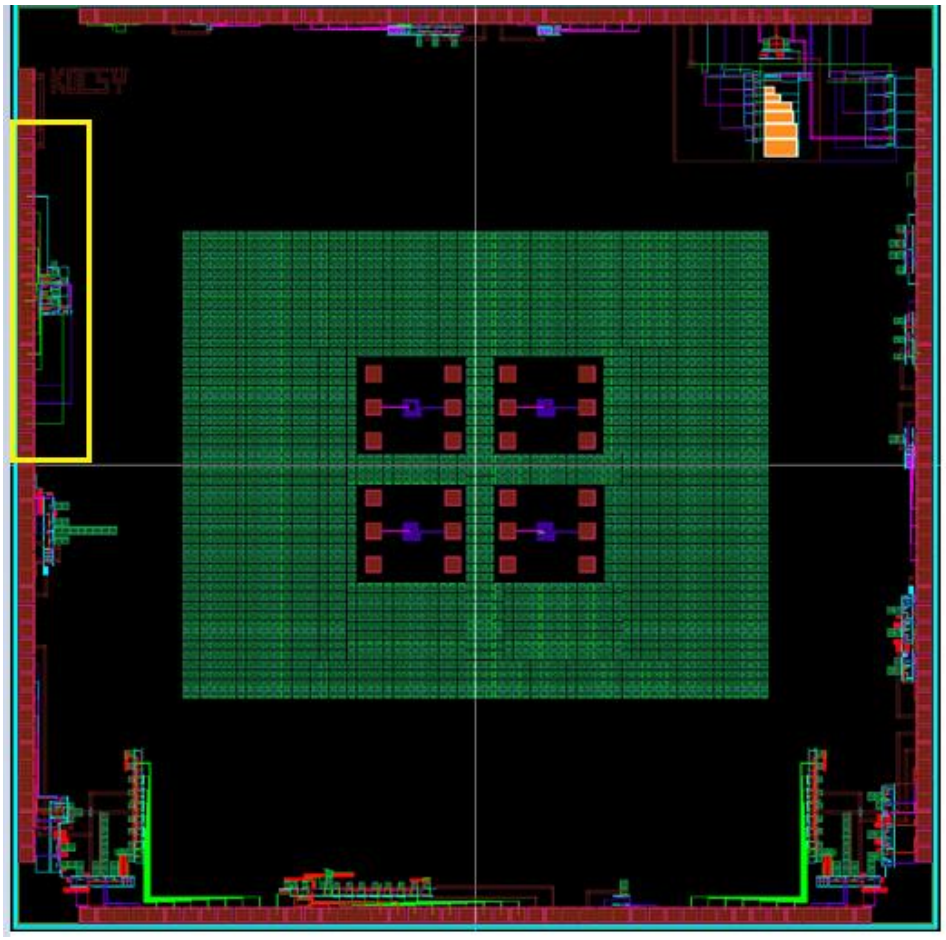

Figure 3-12: Full chip layout. CDS with SCLP filter highlighted in yellow.

The zoomed in display Figure 3-13 occupies an area of 990µm x 216µm with 14 input and output pads.

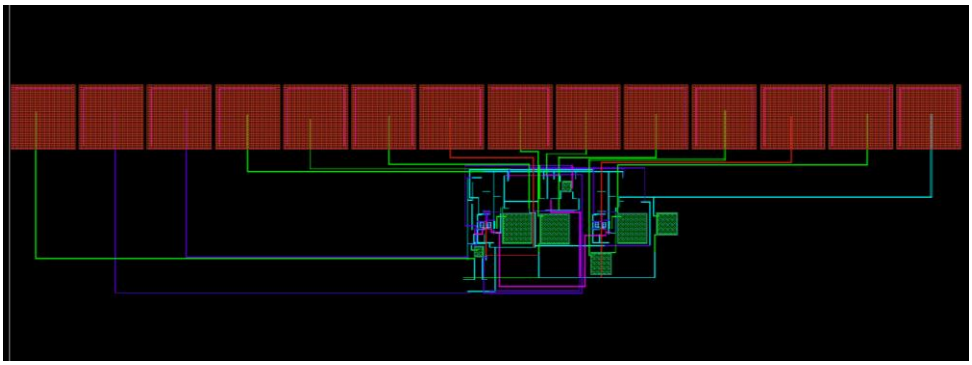

Figure 3-13: Zoomed layout capture of the proposed architecture.

Figure 3-14 is the layout of the proposed architecture that is layout in an area of 990µm x 216µm.

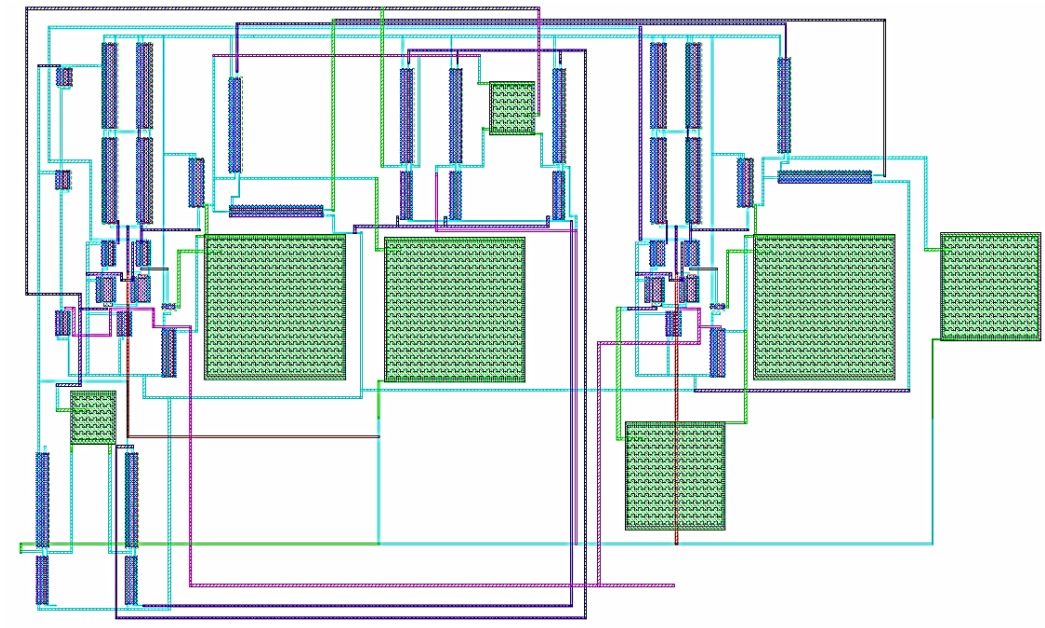

Figure 3-14: layout capture of the proposed architecture.

3.3.2 CORRELATED DOUBLE SAMPLER SIMULATION

The schematics and post extraction simulation are performed with an input range of +1.5V to -1.5V. The corresponding output variation is from +1.5V to -1.5V.

Figure 3-12 is the transient response of CDS with SCLP filter for 500mV, 1V and 1.5V input at 1MHZ clock frequency and 5pF load. Waveform in the order of input sampling clock, charge transfer clock, output sampling clock and output signal. The transient response of the designed correlated double sampler is performed when the CDS is configured with unity gain. An input of 500mV is applied with a sampling frequency of 1MHz and 5pF load capacitance. Figure 3-15 demonstrates that the design can achieve an output voltage of 0.5V.

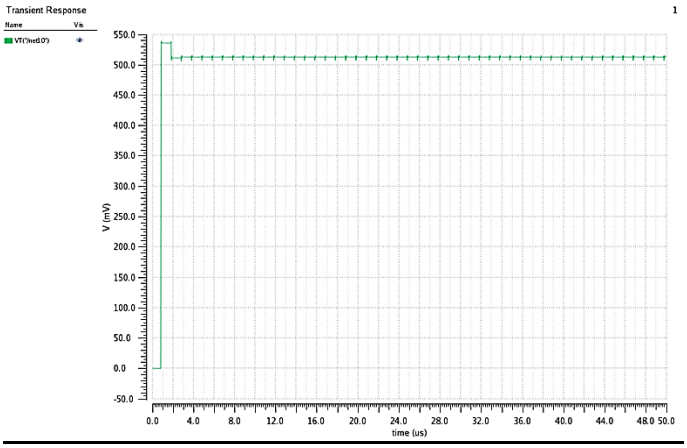

Figure 3-15: transient response for 500mV at the CDS output with 1MHz clock and 5pF load.

Figure 3-15 shows the transient response of the designed correlated double sampler. For transient response the CDS is configured with unity gain. An input of 1V is applied with a

sampling frequency of 1MHz and 5pF load capacitance. It achieves an output voltage of 1V.

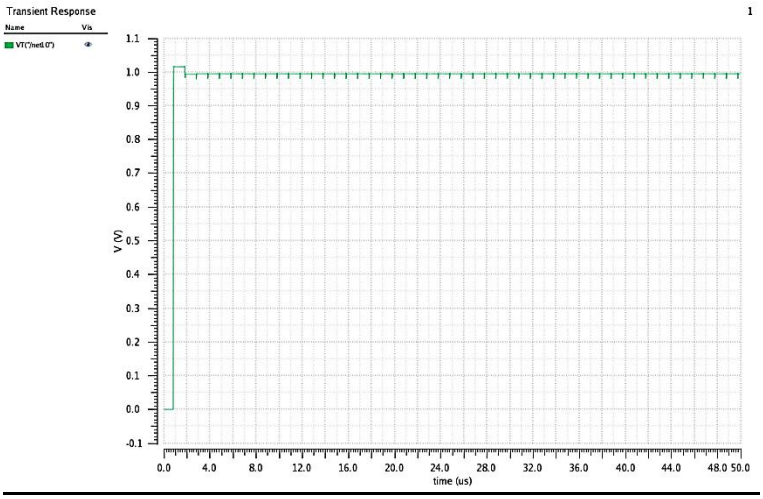

Figure 3-16: transient response for 1V at the CDS output with 1MHz clock and 5pF load.

The same configuration used for the above setups in Figure 3-16 is used to simulate Figure3-17, which is the transient response for -0.5V. An input of -500mV is applied with a sampling frequency of 1MHz and 5pF load capacitance. It achieves an output voltage of -500mV.

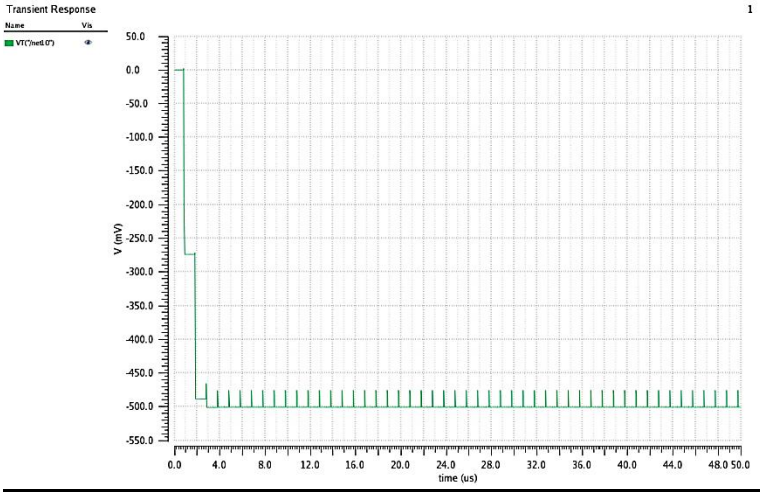

Figure 3-17: transient response for -500mV at the CDS output with 1MHz clock and 5pF load.

An input of -1V is then applied with a sampling frequency of 1MHz and 5pF load capacitance. Figure 3-18 demonstrates the transient response of the designed correlated double sampler. With unity gain feedback configuration an output voltage of -1V is achived.

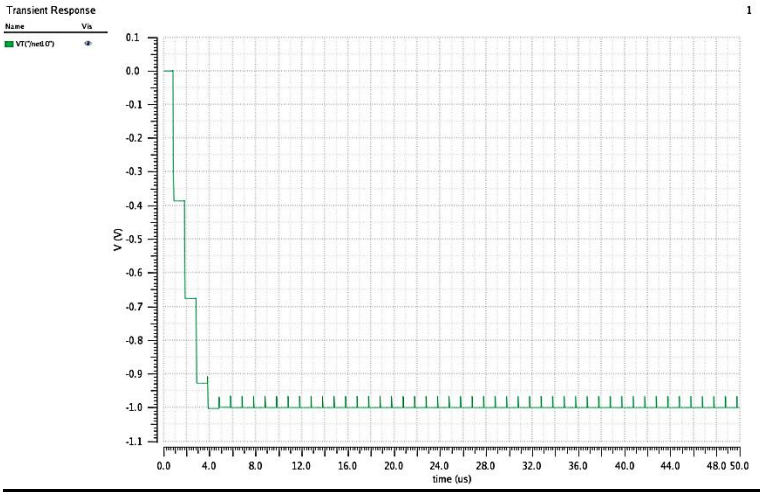

Figure 3-18: transient response for -1V at the CDS output with 1MHz clock and 5pF load.

Figure 3-19 shows the noise response of the designed correlated double sampler. The measurement of noise in the correlated double sampler is done as follows. All the AC input voltages are set to ground potential and the RMS noise is measured at the output of op-amp. Integrating the noise over the frequency range of 1Hz to 20MHz, the RMS output noise of op-amp is calculated to be 1.49µVrms and consumes a power of 60 µW from 3.3V supply.

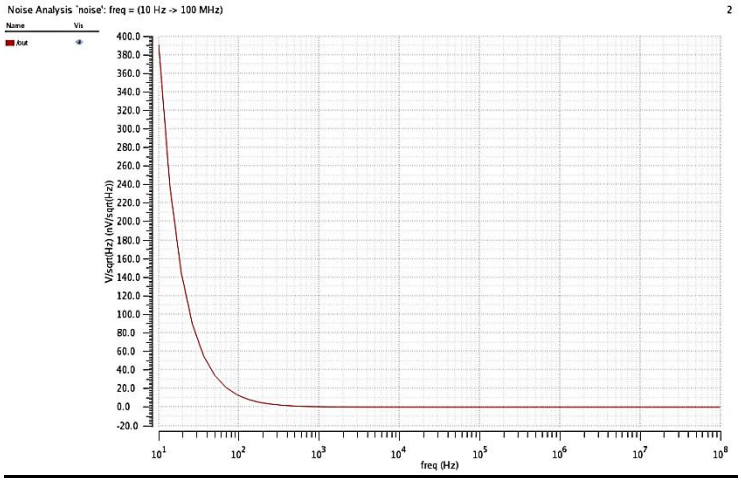

Figure 3-19: output noise of the CDS output noise (µVrms) vs frequency (Hz).

Similar setup used for Figure 3-19 is used for measuring the noise for the correlated double sampler with conventional low pass filter. The AC input voltages are set to zero potential and the RMS noise is measured at the output of op-amp. Figure 3-20 indicates the noise response of the designed correlated double sampler with conventional low pass filter. Integrating the noise over the frequency range of 1Hz to 20MHz, the RMS output noise of op-amp is calculated to be 56µVrms and consumes a power of 170 µW from 3.3V supply.

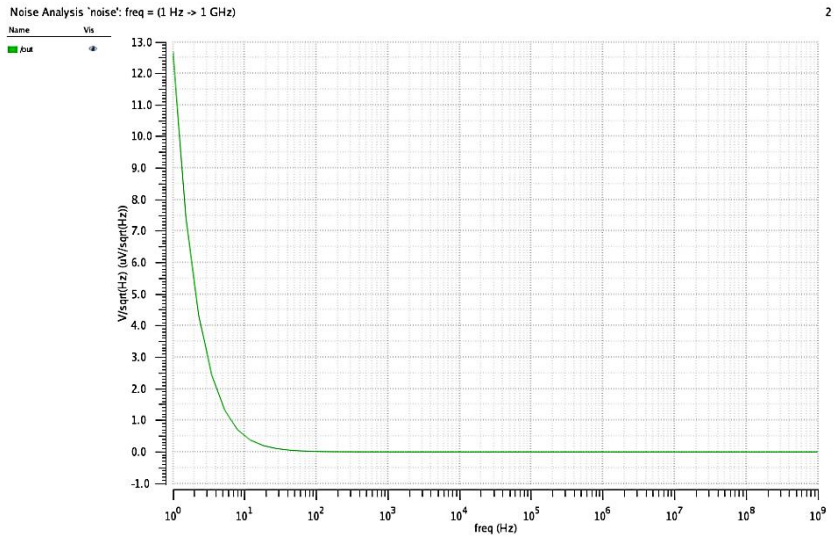

Figure 3-20: output noise of CDS with LP filter output noise (µVrms) vs frequency (Hz).

The overall frequency response of the system is shown in Figure 3-21 the 3dB pole frequency at 2MHz.

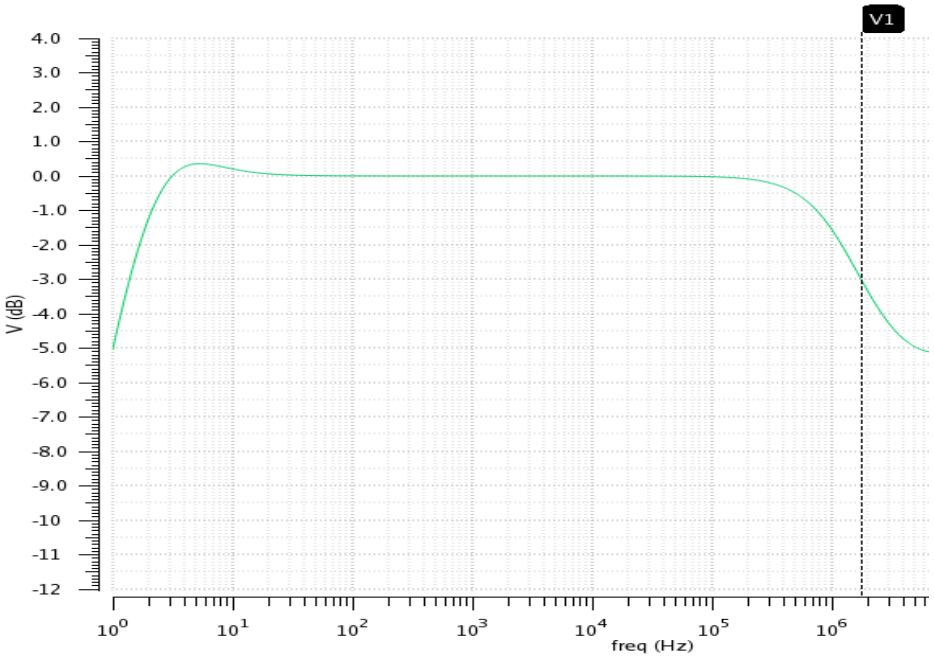

Figure 3-21: Phase response of the overall CDS with SCLP filter system.

Figure 3-22 presents the transient response of the designed novel correlated double sampler with switched capacitor low pass filter. An input of 500mV is applied with a sampling frequency of 1MHz and 5pF load capacitance. There are three clocks Φ1, Φ2 and Φ3 are used in the design operating at 1MHz frequency with a duty cycle ratio of 20%, 70% and 5% respectively. It achieves an output voltage of 500mV.

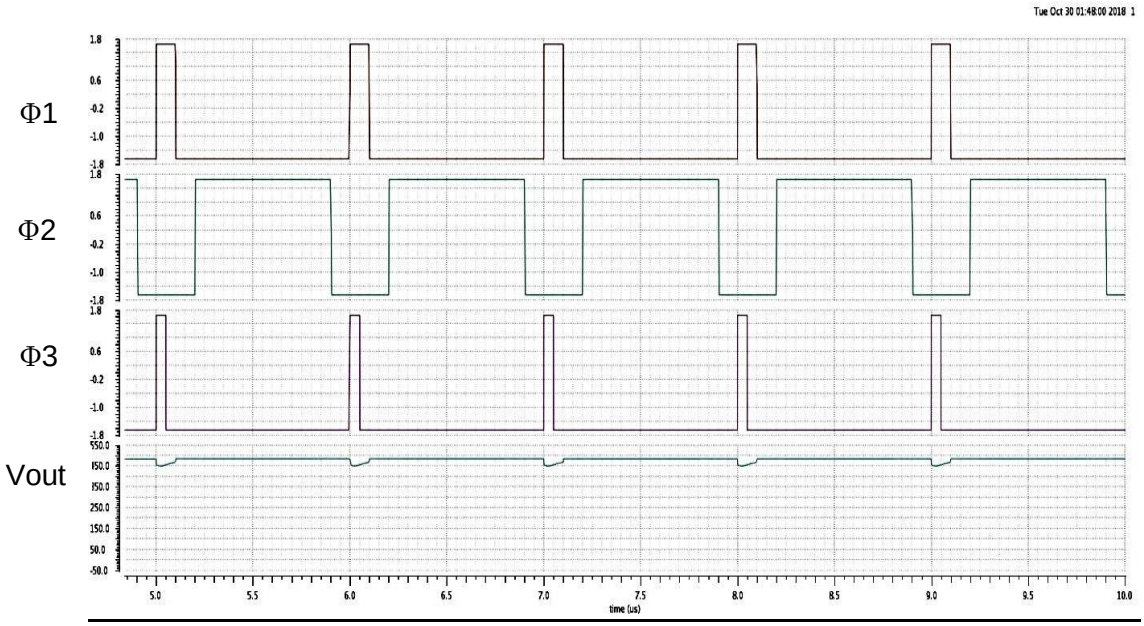

Figure 3-22: transient response for 500mV at the CDS with SCLP filter output with 1MHz clock and 5pF load.

Setup identical to Figure 3-18 used for the 1V simulation. An input of 1V is applied with a sampling frequency of 1MHz and 5pF load capacitance to the proposed correlated double sampler with switched capacitor low pass filter. There are three clocks Φ1, Φ2 and Φ3 are used in the design operating at 1MHz frequency with a duty cycle ratio of 20%, 70% and 5% respectively. It could be seen that from Figure 3-19 the design achieves an output voltage of 1V.

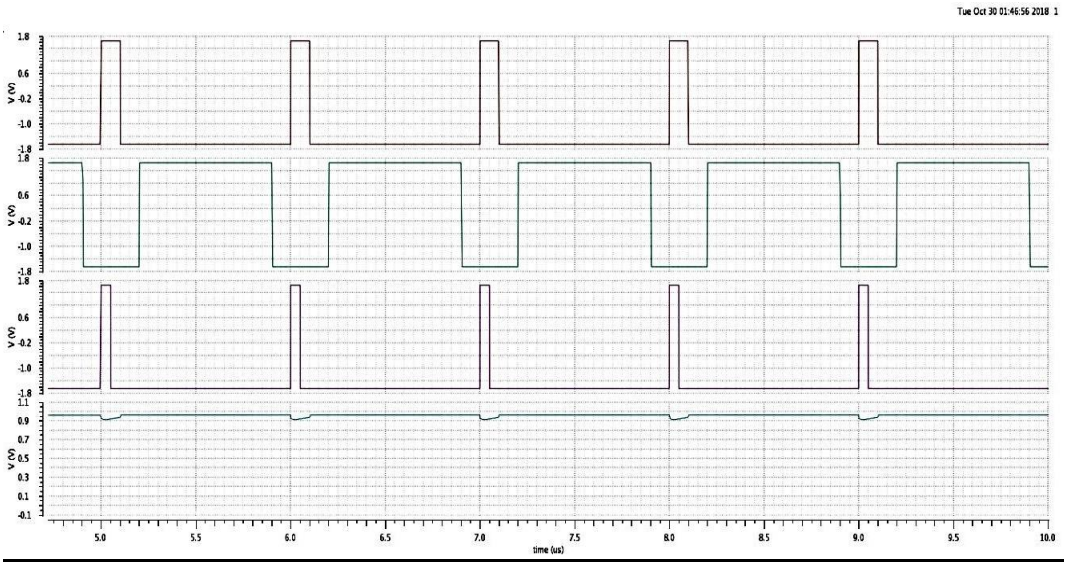

Figure 3-23: transient response for 1V at the CDS with SCLP filter output with 1MHz clock and 5pF load.

Now the input is stepped up to 1.5V with a sampling frequency of 1MHz and maintaining the same 5pF load capacitance. The three clocks Φ1, Φ2 and Φ3 are operated operating at 1MHz frequency with a duty cycle ratio of 20%, 70% and 5% respectively. Figure 3-23 depicts the transient response of the designed novel correlated double sampler with switched capacitor low pass filter achieves an output voltage of 1.5V.

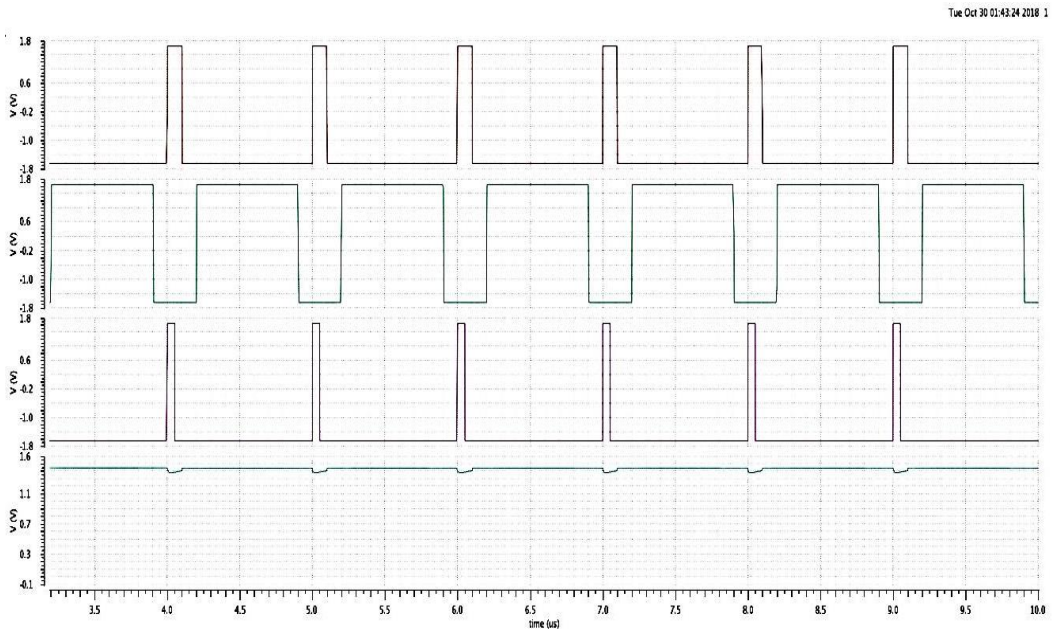

Figure 3-24: transient response for 1.5V at the CDS with SCLP filter output with 1MHz clock and 5pF load.

Figure 3-24 shows the transient response of the new architecture correlated double sampler with switched capacitor low pass filter. An input of -1V is applied with a sampling frequency of 1MHz and 5pF load capacitance. There are three clocks Φ1, Φ2 and Φ3 are used in the design operating at 1MHz frequency with a duty cycle ratio of 20%, 70% and 5% respectively. It achieves an output voltage of -1V.

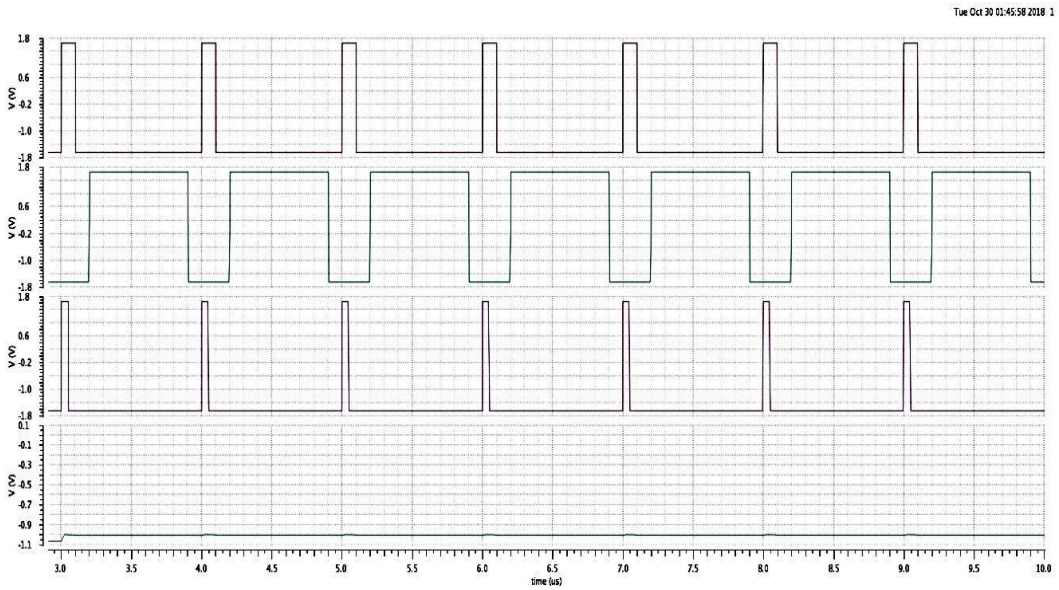

Figure 3-25: transient response for -1V at the CDS with SCLP filter output with 1MHz clock and 5pF load.

Figure 3-25 shows the transient response of the designed novel correlated double sampler with switched capacitor low pass filter. An input of -1.5V is applied with a sampling frequency of 1MHz and 5pF load capacitance. There are three clocks Φ1, Φ2 and Φ3 are used in the design operating at 1MHz frequency with a duty cycle ratio of 20%, 70% and 5% respectively. It achieves an output voltage of -1.5V.

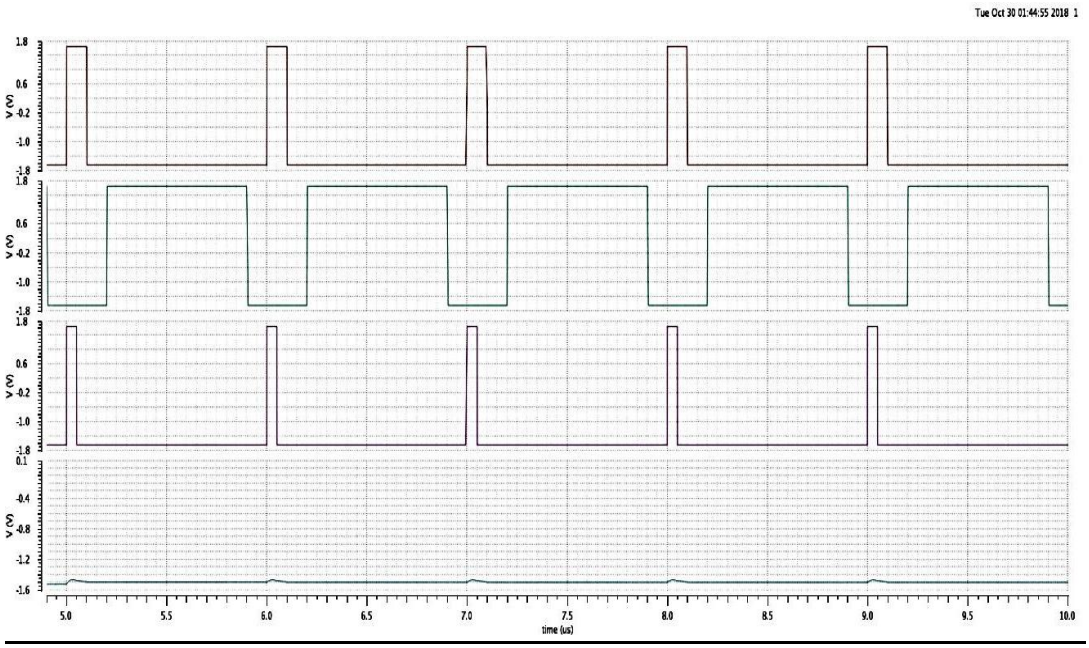

Figure 3-26: transient response for -1.5V at the CDS with SCLP filter output with 1MHz clock and 5pF load.

The overall DC swing of the proposed architecture is captured in Figure 3-26. Where the waveforms are in the order of $\Phi 1$, $\Phi 2$, $\Phi 3$ and V_{out}, with input voltage sweep from -1. 5V to +1.5V the Vout at the CDS with SCLP filter is changing from -1.5V to +1.5V. The sampling clock during the capture is 1MHz and a 5pF load is used.

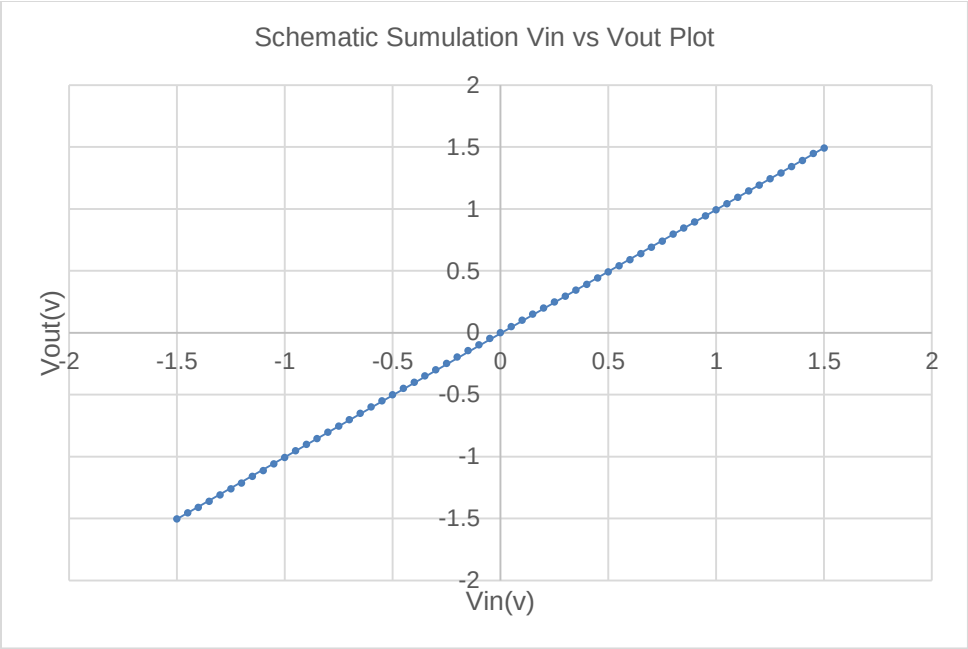

Figure 3-27: linear response of the overall system at the schematics stage.

Figure 3-27: With input sweep from -1. 5V to +1.5V the Vout at the CDS with SCLP filter is following the input from -1. 49V to +1.49V. A 1MHz sampling clock and 5pF load is used. The graph is taken with the 50mV step variation at the Vin of the system.

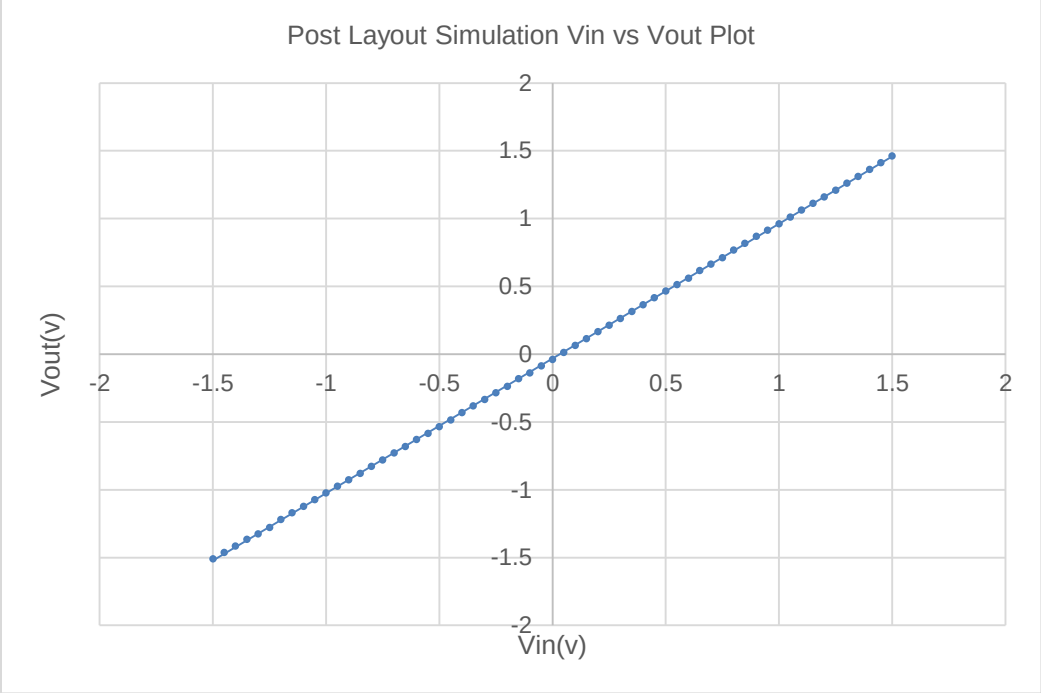

Figure 3-28: linear response of the overall system at the post extraction stage.

The post extraction simulation for the input voltage with respect to the output voltage is shown in figure 3-28. The input is varied with a 50mV step from -1.5V to +1.5V and correspondingly the output voltage is measured.

Figure 3-29 depicts the noise response of the designed correlated double sampler with switched capacitor low pass filter. To measure the noise all the AC input voltages are set to ground potential and the RMS noise is measured at the output of op-amp. Integrating the noise over the frequency range of 1Hz to 20MHz, the RMS output noise of op-amp is calculated to be 0.70µVrms and consumes a power of 124 µW from 3.3V supply.

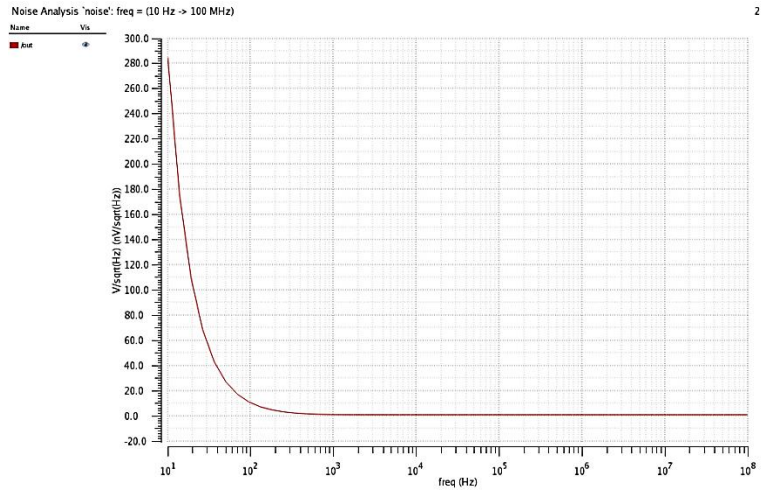

Figure 3-29: output noise of CDS with SCLP filter noise (µVrms) vs frequency (Hz).

The table 3-1 shows the comparison results of all the op-amp architectures that can be used for the pH measurements. With the two-stage telescopic op-amp architecture the noise of 206.8µVrms which is significant. The implementation of correlated double sampler over this op-amp reduces the noise to a radical value of 1.87µVrms. This supports the theory behind the section 3.1.1. To filter out at the output stage a conventional low pass filter is used, this proves an increase in noise floor to 56.76uVrms. This noise produced by the typical low pass filter is drastically reduced by implementing the novel switched capacitor based low pass filter to a value of 0.683µVrms and also an improved power consumption is shown as a result for sampling. This follows the proof that is illustrated in section 3.1.2.

Table 3-2 Post layout simulation results of various architectures

S NO	OP-AMP	CDS	CDS-LP filter	CDS with SC- LP filter
Output Noise	260.8µVrms	1.87µVrms	56.76µVrms	0.683µVrms
Power(uW)	44.105	96.8	171	124.1

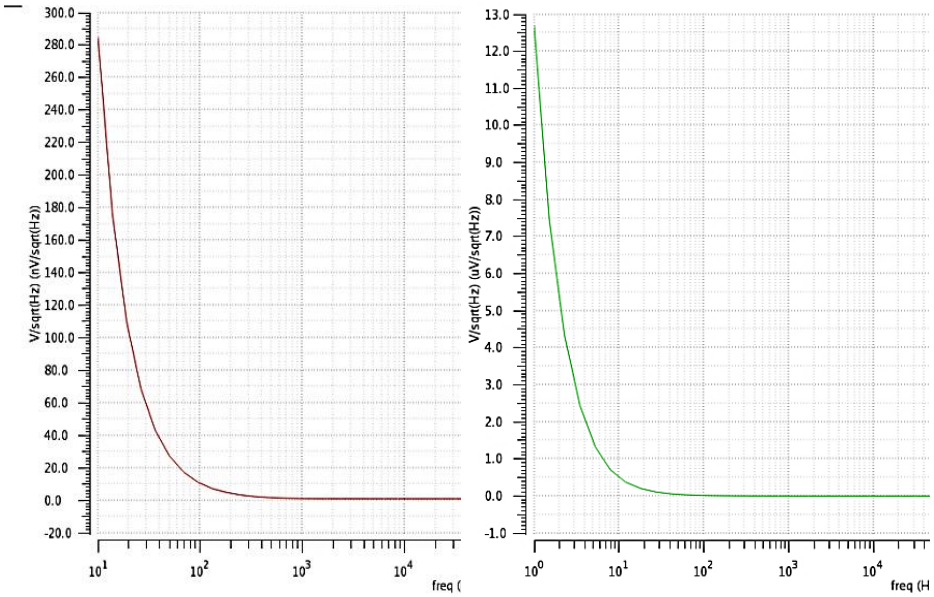

Figure 3-30: Comparison of noise performance between CDS-SCLP and CDS-LP filter.

Figure 3-30 compares the noise performance of the proposed correlated double sampler with switched capacitor low pass filter architecture and the conventional correlated double sampler with low pass filter. The RMS output noise of the proposed circuit is calculated to be 0.70µVrms which is better than the performance of the conventional low pass filter design. The red colored graph corresponds to the noise plot of the proposed architecture and the green colored graph is the conventional architecture's noise plot.

CONCLUSION

This work uses a switched capacitor based low pass filter for the proposed CHEM resistor. The circuit has a linear response for an input range of ±1.5V. The circuit design has two stages. The first stage has a correlated double sampler and the second stage has a switched capacitor based low pass filter. Both the stages operate at 1MHz clock frequency. The first stage alone generates a noise of 1.87µVrms. With low pass filter added at the second stage the op-amp noise added to it and increases the noise to 56.76µVrms. By implementing the low pass filter with the switched capacitor based low pass filter the noise at the lower frequencies are further reduced to 0.683µVrms. The design in implemented in CMOS 0.18µM technology node. The op-amp used in the design is a two-stage telescopic architecture with high gain of 120dB. The capacitive load the circuit can handle is 5pF.

The design is been simulated for various architectures like differential architecture, correlated double sampler, correlated double sampler followed by a low pass filter, and the proposed correlated double sampler followed by a switched capacitor based low pass filter. It is found that the proposed architecture shows significant improvement in reducing the noise. The post layout simulation results show that with a power consumption of 124.1µW the noise is 0.683µVrms.

A comparison between the latest architectures is tabulated in Table 4-1. The Instrumentation amplifier with programmable gain is used for bio potential application[25] with the supply is 0.5V. This justifies the low power consumption of the device, but the noise produced is still high.

Switched capacitor based trans-impedance amplifier [22] with a sampling of 100 kHz and 3V supply proposes that the noise and power are low. The input transistors are operated in week inversion region for reducing the power and noise. Sub threshold region or week inversion region claims to have process issues and the performance would change based on the fabrication process deviation also this would increase the cost of the DIE. The next resent implementation of potentiometric circuit for biomedical application is a 1V 2.3 µW biomedical signal acquisition [35]. Here the transistors are operated in sub threshold region with a 1V supply range. Considering the region of operation and supply range the noise seen at the output is really high. The same hold true for the following architecture a 1V 1.1 µW sensor interface IC for biomedical devices [36].

In pH sensing applications a low noise low power DC coupled sensor amplifier with offset cancellation [37] architecture consumes a reasonable low power and low noise but still there are areas of improvement in noise and power. The latest potentiometric readout with CVCC [26] method is used pH sensing application, were there is huge power consumption which is not suitable for the in-vivo applications. This holds true for the Wearable electronic sensor for potentiometric application [38]. In both the cases the noise seen at the output of the circuit is really high.

With all the architectures shown in the table 4-1 there are architectures compromising between either noise or power, where the transistors are operated in subthreshold region and the power supply is compromised to achieve low power. Also, the pH sensing applications have not achieved any significant improvement in the power or noise which is not suitable for in-vivo application.

Table 4-1 Architecture comparison

Architecture	Power consumption	Noise	Complexity	Application
Instrumentation amplifier with programmable gain [25]	1.1µW	1.15µVrms	Moderate	Electro-cardio gram
Switched capacitor based trans-impedance amplifier at 100 kHz [22]	15.174µW	2.89µVrms	Moderate	Electro-cardio gram
A 1V 2.3µW Biomedical Signal Acquisition[35]	2.3 µW	2.1µVrms	Moderate	Electro-cardio gram
A 1-V 1.1-µW Sensor Interface IC for Wearable Biomedical Devices[36]	1.3µW	2.1µVrms	Moderate	Electro-cardio gram
A Low Noise Low Power DC Coupled Sensor Amplifier with Offset Cancellation[37]	900µW	991.1µVrms	Moderate	pH sensing
Potentiometric readout with CVCC method [26]	1.3mW	NA	Moderate	pH sensing
Wearable Electronic Sensor for Potentiometric[38]	500mW	NA	Complex	pH sensing
CDS with SC- LP filter (This work)	124.1µW	0.683µVrms	Moderate	pH sensing

Finally, this work has the interface with pH sensor that can be used for any sensor application with DC output ranging from -1.5V to +1.5V which operates with a 3.3V supply could achieve 0.683µVrms and 124µW power. This proves that the proposed switched capacitor based low pass filter can achieve low RMS noise with most accurate measurement from the sensor.

REFERENCES

[1] Tae Hoon Lee, Gyuseong Cho, Hee Joon Kim, Seung Wook Lee, Wanno Lee and Sang Hyo Han, "Analysis of 1/f noise in CMOS preamplifier with CDS circuit," 2001 IEEE Nuclear Science Symposium Conference Record (Cat. No.01CH37310), San Diego, CA, USA, 2001, pp. 792-796 vol. 2, 2001.

[2] "A Potentiometric Sensor System with Integrated Circuitry for in situ Environmental Monitoring - IEEE Conference Publication", *Ieeexplore.ieee.org*, 2018.

[3] B. Rodrigues, A. Siarkowski, O. Sagazan, S. Crand, T. Mohammed-Brahim and N. Morimoto, "Sensors based in suspended gate field effect transistors for pH measurements", *Journal of Physics: Conference Series*, vol. 421, p. 012006, 2013.

[4] R. Shideler and U. Bertocci, "A low-noise potentiostat for the study of small amplitude signals in electrochemistry", *Journal of Research of the National Bureau of Standards*, vol. 85, no. 3, p. 211, 1980.

[5]A. Dybko, "CHEMICAL SENSORS RESEARCH GROUP", *Csrg.ch.pw.edu.pl*, 2018.

[6] C. Huang, "Design of a Portable Potentiostat with Dual-microprocessors for Electrochemical Biosensors", *Universal Journal of Electrical and Electronic Engineering*, vol. 3, no. 6, pp. 159-164, 2015.

[7] M. Steyaert and W. Sansen, "A micropower low-noise monolithic instrumentation amplifier for medical purposes", *IEEE Journal of Solid-State Circuits*, vol. 22, no. 6, pp. 1163-1168, 1987.

[8] R. Harrison and C. Charles, "A low-power low-noise cmos for amplifier neural recording applications", *IEEE Journal of Solid-State Circuits*, vol. 38, no. 6, pp. 958-965, 2003.

[9] Y. Chin, J. Chou, T. Sun, W. Chung and S. Hsiung, "A novel pH sensitive ISFET with on chip temperature sensing using CMOS standard process", *Sensors and Actuators B: Chemical*, vol. 76, no. 1-3, pp. 582-593, 2001.

[10] A. van den Berg, P. Bergveld, D. Reinhoudt and E. Sudhölter, "Sensitivity control of ISFETs by chemical surface modification", 2018. .

[11] S. Martinoia and G. Massobrio, "A behavioral macromodel of the ISFET in SPICE", *Sensors and Actuators B: Chemical*, vol. 62, no. 3, pp. 182-189, 2000.

[12] W. Gui-Hua, Y. Dun and W. Yao-Lin, "ISFET temperature characteristics", *Sensors and Actuators*, vol. 11, no. 3, pp. 221-237, 1987.

[13] N. Moser, T. S. Lande, C. Toumazou and P. Georgiou, "ISFETs in CMOS and Emergent Trends in Instrumentation: A Review," in *IEEE Sensors Journal*, vol. 16, no. 17, pp. 6496-6514, Sept.1, 2016.

[14] T. Yoshida, M. Akagi, M. Sasaki and A. Iwata, "A 1V supply successive approximation ADC with rail-to-rail input voltage range," *2005 IEEE International Symposium on Circuits and Systems*, Kobe, Vol. 1, pp. 192-195, 2005.

[15] M. Yin and M. Ghovanloo, "A Low-Noise Preamplifier with Adjustable Gain and Bandwidth for Biopotential Recording Applications," *2007 IEEE International Symposium on Circuits and Systems*, New Orleans, LA, pp. 321-324, 2007.

[16] J. R. Blanco *et al*., "Design of a Low-Cost Portable Potentiostat for Amperometric Biosensors," *2006 IEEE Instrumentation and Measurement Technology Conference Proceedings*, Sorrento, pp. 690-694, 2006.

[17] M. F. Abdullah *et al*., "A comparative study on low noise precision difet operational amplifier and low noise operational amplifier for potentiometric transduction circuit," *2013*

IEEE Business Engineering and Industrial Applications Colloquium (BEIAC), Langkawi, pp. 584-588, 2013.

[18] M. F. Abdullah *et al*., "A miniaturization using Surface Mount Technology of potentiometric indicator system for measuring human stress," *2012 IEEE Symposium on* Industrial Electronics and Applications, Bandung, pp. 67-71, 2012.

[19] P. Bembnowicz, G. Yang, S. Anastasova, A. Spehar-Délèze and P. Vadgama, "Wearable electronic sensor for potentiometric and amperometric measurements," *2013 IEEE International Conference on Body Sensor Networks*, Cambridge, MA, USA, pp. 1-5, 2013.

[20] S. Maréchal, O. Nys, F. Krummenacher, M. Chevroulet and M. Kayal, "A continuous-time instrumentation amplifier employing a novel auto-zeroing structure," *Proceedings of the 20th International Conference Mixed Design of Integrated Circuits and Systems - MIXDES 2013*, Gdynia, pp. 157-162, 2013.

[21] C. C. Enz and G. C. Temes, "Circuit techniques for reducing the effects of op-amp imperfections: autozeroing, correlated double sampling, and chopper stabilization," in *Proceedings of the IEEE*, vol. 84, no. 11, pp. 1584-1614, Nov. 1996.

[22] D. Dubey and A. Gupta, "A low power low noise amplifier for biomedical applications," *2015 IEEE International Conference on Electrical, Computer and Communication Technologies (ICECCT)*, Coimbatore, pp. 1-6, 2015.

[24] W. Chung *et al*., "An implementation of an electronic tongue system based on a multi-sensor potentiometric readout circuit with embedded calibration and temperature compensation," *2015 IEEE SENSORS*, Busan, pp. 1-4, 2015.

[25] M. K. Adimulam, A. Divya, K. Tejaswi and M. B. Srinivas, "A low power, low noise Programmable Analog Front End (PAFE) for biopotential measurements," *2017 39th Annual International Conference of the IEEE Engineering in Medicine and Biology Society (EMBC)*, Seogwipo, pp. 3844-3847, 2017.

[26] W. Chung *et al*., "Design of a multi-sensor readout chip for amperometric, potentiometric, impedometric, and colorimetric bio-sensor applications," *2017 International Conference on Applied System Innovation (ICASI)*, Sapporo, pp. 806-809, 2017.

[27] Y. Chin, J. Chou, T. Sun, W. Chung and S. Hsiung, "A novel pH sensitive ISFET with on chip temperature sensing using CMOS standard process", Sensors and Actuators B: Chemical, vol. 76, no. 1-3, pp. 582-593, 2001.

[28] W. Chung, Y. Lin, D. Pijanowska, C. Yang, M. Wang, A. Krzyskow and W. Torbicz, "New ISFET interface circuit design with temperature compensation", *Microelectronics Journal*, vol. 37, no. 10, pp. 1105-1114, 2006.

[29] M. Belloni, E. Bonizzoni, A. Fornasari and F. Maloberti, "A Micropower Chopper—CDS Operational Amplifier", *IEEE Journal of Solid-State Circuits*, vol. 45, no. 12, pp. 2521-2529, 2010.

[30] Y. Park, C. Kim, B. Jung, H. Yoo and H. Ko, "Low Noise and Low Power IC Using Opamp Sharing Technique for Capacitive Micro-Sensor Sensing Platform", *Journal of Sensor Science and Technology*, vol. 26, no. 1, pp. 60-65, 2017.

[31] B. RAZAVI, "Design of Analog CMOS Integrated Circuits,Solutions(McGraw) - RAZAVI", *Scribd*, 2018.

[32] W. Chung, A. Silverio, V. Tsai, C. Cheng, S. Chang, Z. Ming-Ying, C. Kao, S. Chen, D. Pijanowska, D. Rustia and Y. Lo, "An implementation of an electronic tongue system based on a multi-sensor potentiometric readout circuit with embedded calibration and temperature compensation", 2018. .

[33] P. Bergveld, "Thirty years of ISFETOLOGY", *Sensors and Actuators B: Chemical*, vol. 88, no. 1, pp. 1-20, 2003.

[34] W. Chung, A. Silverio, V. Tsai, C. Cheng, S. Chang, Z. Ming-Ying, C. Kao, S. Chen, D. Pijanowska, D. Rustia and Y. Lo, "An implementation of an electronic tongue system based on a multi-sensor potentiometric readout circuit with embedded calibration and temperature compensation", *Microelectronics Journal*, vol. 57, pp. 1-12, 2016.

[35] T. Farouk, M. Elkhatib and M. Dessouky, "A 1V low-power low-noise bio potential amplifier based on flipped voltage follower," 2015 IEEE International Conference on Electronics, Circuits, and Systems (ICECS), Cairo, pp. 539-542 , 2015.

[36] Xiaodan Zou, Xiaoyuan Xu, Jun Tan, Libin Yao and Yong Lian, "A 1-V 1.1-μW sensor interface IC for wearable biomedical devices," IEEE International Symposium on Circuits and Systems, Seattle, WA, pp. 2725-2728, 2008.

[37] H. K. Krishnamurthy, D. Robinson, D. M. Rector and G. S. La Rue, "A Low Noise Low Power DC Coupled Sensor Amplifier with Offset Cancellation," 2010 IEEE Workshop on Microelectronics and Electron Devices, Boise, ID, pp. 1-4, 2010.

[38] P. Bembnowicz, G. Yang, S. Anastasova, A. Spehar-Délèze and P. Vadgama, "Wearable electronic sensor for potentiometric and Amperometric measurements," 2013 IEEE International Conference on Body Sensor Networks, Cambridge, MA, USApp. 1-5, 2013.

[39] Fundamentals of Electrochemistry, 2nd edition. Viladimir S. Bagotsky. ISBN: 978-0-471-70058-6, Nov 2005.

BIOGRAPHICAL INFORMATION

Revathy Perumalsamy is a candidate for the Master of Science degree at the University of Texas at Arlington. She received his Bachelor's degree in Electronics & Instrumentation Engineering from Anna University in India and worked in HCL Technologies and Tessolve services PVT Ltd and Business Solutions Limited in India until August 2016 as Test engineer in the area of automotive electronics. In 2016 fall, she joined the AMIC lab under the supervision of Dr. Sungyong Jung to design, integrate and test, systems and circuits for electrochemical sensors. During his Master's she has interned in spring 2018 at Texas Instruments as engineer intern of high speed OPAMP. As test engineer she performed qualification of OPAMPS and involved in designing test boards for OPAMPS.